Journal of Medicinal Chemistry

Article

The Discovery of 3-((4-Chloro-3-methoxyphenyl)amino)-1-((3R,4S)-4-cyanotetrahydro-2H-pyran-3-yl)-1H-pyrazole-4-carboxamide, a Highly Ligand Efficient and Efficacious JAK1 Selective Inhibitor with Favorable Pharmacokinetic Properties

Tony Siu, Jason Brubaker, Peter Fuller, Luis Torres, Hongbo Zeng, Joshua Close, Dawn M Mampreian, Feng Shi, Duan Liu, Xavier Fradera, Kevin Johnson, Nathan Bays, Elma Kadic, Fang He, Peter Goldenblatt, Lynsey Shaffer, Sangita B Patel, Charles A Lesburg, Carla Alpert, Lauren Dorosh, Sujal V Deskmukh, Hongshi Yu, Joel Klappenbach, Fiona Elwood, Christopher J. Dinsmore, Rafael Fernandez, Lily Moy, and Jonathan R Young

J. Med. Chem., **Just Accepted Manuscript** • DOI: 10.1021/acs.jmedchem.7b01135 • Publication Date (Web): 20 Nov 2017

Just Accepted

ACS Publications

Journal of Medicinal Chemistry is published by the American Chemical Society. 1155 Sixteenth Street N.W., Washington, DC 20036

The Discovery of 3-((4-Chloro-3-methoxyphenyl)amino)-1-((3R,4S)-4-cyanotetrahydro-2H-pyran-3-yl)-1H-pyrazole-4-carboxamide, a Highly Ligand Efficient and Efficacious JAK1 Selective Inhibitor with Favorable Pharmacokinetic Properties

Tony Siu[a]*, Jason Brubaker[a], Peter Fuller[a], Luis Torres[a], Hongbo Zeng[a], Joshua Close[a], Dawn M. Mampreian[a], Feng Shi[k], Duan Liu[b], Xavier Fradera[c], Kevin Johnson[h], Nathan Bays[d], Elma Kadic[d], Fang He[l], Peter Goldenblatt[d], Lynsey Shaffer[d], Sangita B. Patel[e], Charles A. Lesburg[e], Carla Alpert[d], Lauren Dorosh[d], Sujal V. Deskmukh[f], Hongshi Yu[g], Joel Klappenbach[h], Fiona Elwood[j], Christopher J. Dinsmore[a], Rafael Fernandez[d], Lily Moy[i], and Jonathan R. Young[a]

Departments of [a]Medicinal Chemistry, [b]Discovery Process Chemistry, [c]Modeling & Informatics, [d]In Vitro Pharmacology, [e]Structural Chemistry, [f]Pharmacokinetics Pharmacodynamics and Drug Metabolism, [g]Discovery Pharmaceutical Sciences, [h]Molecular Biomarkers, [i]In Vivo Pharmacology, [j]Respiratory and Immunology, Merck & Co., Inc., 33 Avenue Louis Pasteur, Boston, MA 02115 USA

[k]Department of Chemistry, Pharmaron Beijing Co. Ltd.
6 Taihe Road
BDA, Beijing, 100176
P.R. China

[l]Department of Biology, Pharmaron Beijing Co. Ltd.
6 Taihe Road
BDA, Beijing, 100176
P.R. China

Abstract

The discovery of a potent selective low dose JAK1 inhibitor suitable for clinical evaluation is described. As

part of an overall goal to minimize dose, we pursued a medicinal chemistry strategy focused on optimization of key parameters that influence dose size, including lowering human Cl_{int} and increasing intrinsic potency, bioavailability, and solubility. To impact these multiple parameters simultaneously, we used lipophilic ligand efficiency as a key metric to track changes in the physicochemical properties of our analogs, which led to improvements in overall compound quality. In parallel, structural information guided advancements in JAK1 selectivity by informing on new vector space, which enabled the discovery of a unique key amino acid difference between JAK1 (Glu966) and JAK2 (Asp939). This difference was exploited to consistently produce analogs with the best balance of JAK1 selectivity, efficacy, and projected human dose, ultimately culminating in the discovery of compound **28**.

Introduction

The Janus Kinase-Signal Transducer and Activator of Transcription (JAK-STAT) pathway is a well-studied signaling pathway that regulates cytokine and growth factor production.[1] Signaling in this pathway is mediated by four tyrosine kinases including JAK 1, 2, and 3, as well as non-receptor tyrosine-protein kinase 2 (TYK2). These cytoplasmic JAK isoforms are associated with cytokine receptors as homo and hetero dimers and trimers. Upon activation through cross phosphorylation, they recruit and phosphorylate STAT transcription factors, which translocate to the nucleus and activate gene transcription. Impressively, only four JAK isoforms are needed to regulate the vast number of signaling cytokines including interferons, interleukins, endocrine factors, and growth factors. These cytokines regulate a host of biological functions including T and B cell activation and differentiation, inflammation, and hemopoiesis. The JAK-STAT pathway has a vast role in regulating crucial cellular events and is a key contributor to and extensively linked with immune and malignant-related diseases.[2]

Rheumatoid arthritis (RA) is an autoimmune disease characterized by inflammation of the synovial membrane of joints.[3] RA associated inflammation leads to severe joint pain along with stiffness and over time chronic inflammation leads to destruction of the joint and loss of function. Central to the pathogenesis of RA is the inflammatory function of immune cells that are coordinated and maintained by cytokines

regulated by the JAK family of kinases. To combat the inflammatory etiology of the disease, there are commercial therapies that target both the cytokines (*e.g.* anti-TNFα agents, infliximab and entanercept) and the JAK pathway (*e.g.* pan-JAK inhibitor, tofacitinib (**1**), Figure 1).[4] Despite the success of these safe and efficacious treatments, an unmet medical need still remains for safe small molecule disease modifying anti-rheumatic drugs (DMARDS) that can achieve greater efficacy and provide more convenience than the current therapies.[5] However, a limiting factor for achieving greater efficacy with tofacitinib is the dose limiting anemia observed in clinical trials which is associated with JAK2 inhibition and its effects on erythropoiesis.[4a] These data suggest that an inhibitor selective for JAK1 over JAK2 may offer greater clinical benefit by increasing the therapeutic margin over erythropoietin (EPO) inhibition. A key assumption in this approach is that JAK1 inhibition alone is sufficient to achieve similar anti-inflammatory efficacy as pan-JAK inhibition. A distinct challenge to develop JAK1 selective inhibitors is the high sequence homology between JAK1 and JAK2 in the catalytic domain. Despite these challenges, numerous research groups have reported their strategies and progress in this area.[6]

In this paper we describe our strategy towards the identification of a small molecule JAK1 selective inhibitor with drug-like properties and low projected human dose. Due to the differences in K_M values for ATP in the various JAK isoforms, the most relevant measurement of isoform selectivity is to differentiate against tofacitinib on key pathways of efficacy (*e.g.* interleukin-6 (IL-6)) relative to anemia (*e.g.* EPO). By differentiating compound selectivity using cell-based assays, we sought to improve the potential for clinical translation of efficacy over anemia. Recently, we disclosed pyrazole carboxamide **2** as a potent JAK1 selective tool compound with a modest 10-fold selectivity over JAK2 in both enzymatic and pathway cell-based assays (Figure 1).[7] As a proof of concept, compound **2** demonstrated a larger therapeutic window over tofacitinib in the collagen induced arthritis (CIA) efficacy and reticulocyte anemia models.[8] These initial efforts supported the strategy that selectivity for the IL-6 pathway through JAK1 inhibition is sufficient to achieve efficacy while sparing anemia bio-markers.

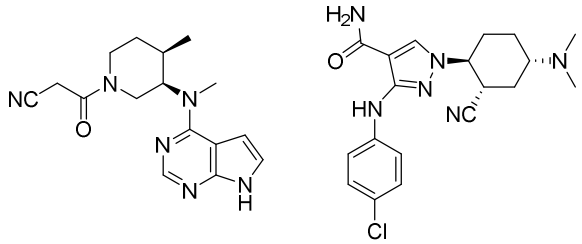

1 **2**

Compound	**1** (tofacitinib)	**2**
JAK1 IC_{50} (nM)[a]	1.3	1.5
JAK2 IC_{50} (nM)[a]	1.4	19
JAK3 IC_{50} (nM)[a]	0.34	1226
TYK2 IC_{50} (nM)[a]	12	13
Cell IL6 IC_{50} (nM)[b]	124	64
Cell EPO IC_{50} (nM)[b]	107	692
Ratio EPO/IL6	0.86	11

Figure 1. Selectivity profile for tofacitinib **1** and **2.** [a]Values in this table were determined by the HTRF assay and are the mean of n = 2 experiments. [b]Values in this table are determined by GeneBLAzer assay and are the mean of n = 2 experiments.

While achieving our goal of a pathway JAK1 selective inhibitor, extensive characterization of **2** revealed a high human predicted daily dose (343 mg QD) and a potential hERG liability (Figure 2).[9] Minimizing the daily dose reduces body burden and the risk for idiosyncratic toxicities as well as improves patient compliance.[10] Furthermore, the high dose of **2** resulted in a relatively high dose number (D_0 = 80), which often complicates formulation options and risk assessment for clinical compounds.[11]

hERG Activity of Compound **2**	Predicted Human Dose of Compound **2**
MK499 IC_{50} = 12,200 nM Patch Clamp IC_{50} = 3000 nM CV Guinea Pig QT NOEL: 8x over predicted clinical C_{max}	r; h Hept Cl_{int} (mL/min/kg) = 109; 26 Rat Cl_p = 41 mL/min/kg Vd_{ss} = 11 L/kg F% = 16 Dog Cl_p = 21 mL/min/kg Vd_{ss} = 8 L/kg F% = 42 Predicted Human Dose = 343 mg QD D_0 = 80

Figure 2. Characterization and liabilities of compound **2.**

Considering the potential issues with a high daily dose drug and the need for enabled formulation, our goal in the current effort was to identify a lead candidate with predicted daily dose ≤ 100 mg while decreasing D_0. To optimize for a lower dose of an AUC driven target, we focused on the key parameters of intrinsic clearance (Cl_{int}) and unbound AUC (AUC_u), fraction absorbed (f_a), and fraction escaping gut metabolism (f_g), whose relations is expressed by the equation in Figure 3.[12] Thus, reduction of the dose of **2** required decreasing human Cl_{int} and AUC_u (by increasing intrinsic potency), as well as increasing f_a through improvements in solubility and permeability.

$$\text{Dose} = \frac{AUC_u \times CL_{int}}{fa * fg}$$

Figure 3. Parameters that affect human dose calculation for AUC driven protein target. AUC unbound (AUC_u), intrinsic clearance (Cl_{int}), fraction absorbed (f_a), fraction escape from gut metabolism (f_g).

In addition to the high daily dose of compound **2,** modest affinity for the hERG channel (MK499 IC_{50} = 12,200 nM) was confirmed in the functional patch clamp hERG blockade assay (hERG IC_{50} = 3,000 nM).[13] Ultimately, the unacceptable safety margin for QTc prolongation shown in a guinea pig study (8 fold margin over predicted human Cmax) combined with its high daily dose precluded **2** from further progression.[14] Blockade of the hERG channel has the potential to alter the QT interval and trigger life threatening tosades des pointes, therefore further optimization was necessary to identify a suitable clinical candidate.[15]

Results and Discussion

Initial strategies for reducing hERG channel binding focused on applying destabilizing SAR derived from the 3D QSAR model for hERG channel activity.[16] This strategy included structural modifications including removing or attenuating the basicity of the most basic amine in **2** as well as increasing overall polarity of the inhibitor. These approaches successfully led to multiple SAR advances resulting in weakened hERG binding, but unfortunately negatively impacted other dose related parameters which hindered progress (Figure 4). Replacing the basic amine with a hydroxyl group (*e.g.* compound **3**) led to improved MK499 (IC_{50} = 26,000 nM) while maintaining intrinsic potency (JAK1 IC_{50} = 1.2 nM), but the bioavailability was compromised (F% =10). A similar effect on hERG binding was achieved through steric hindrance by shielding the basic amine with methyl oxetane (*e.g.* compound **4)** (MK499 IC_{50} = 46,000 nM, JAK1 IC_{50} = 0.6 nM) but did not improve the Cl_{int} compared to **2**, presumably due to the increased lipophilic

substituents compared to **2**. Maintaining the basic amine while increasing the overall polarity of the compound (*e.g.* compound **5** (HPLC Log D = 1.54 vs. 2.15 for compound **2**) MK499 IC_{50} = 32,000 nM, JAK1 IC_{50} = 0.3 nM) improved the hERG signal, albeit with negative impacts on cellular permeability and overall fraction absorbed when dosed orally. The team explored many SAR permutations to balance hERG binding, Cl_{int}, and bioavailability, but ultimately failed to deliver compounds with the required balance profile within the compound **2** chemotype.

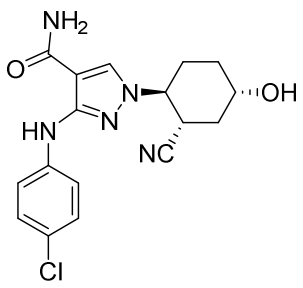

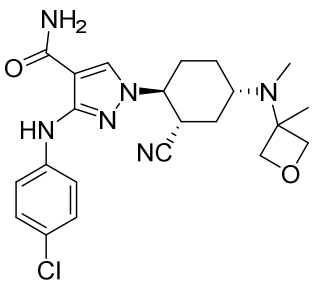

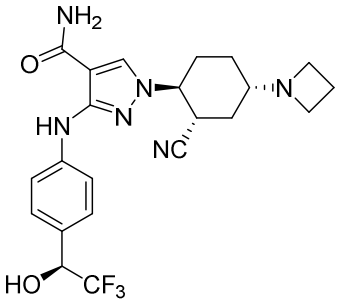

3	**4**	**5**
Basic Amine Replacement JAK1 IC_{50} = 1.2 nM MK499 IC_{50} = 26000 nM	**Hindered Amine** JAK1 IC_{50} = 0.6 nM MK499 IC_{50} = 46000 nM	**Increased Polarity** JAK1 IC_{50} = 0.3 nM MK499 IC_{50} = 32000 nM
Poor Bioavailability Rat F% = 10	**High Intrinsic Cl_{int}** r;h Hept Cl_{int} = 80;32 mL/min/kg	**Low Permeability** Papp = 3.3 x 10^{-6} cm/sec Rat F% = 0

Figure 4. Strategies to address hERG binding negatively impacted dose-relate parameters

Although compound **2** possessed adequate properties to achieve proof of concept and demonstrate in vivo functional selectivity, the challenges around modification of the basic amine to attenuate hERG and lower dose motivated the team to remove the amine entirely. This led to the identification of truncated compound **6** with high ligand binding efficiency (LBE = 0.50).[17] Removal of the basic amine completely ablated hERG binding activity and provided an encouraging starting point for optimization despite relatively high clearance parameters (Figure 5). As such, the team embarked on a design strategy to simultaneously optimize multiple parameters by improving the physicochemical properties while maintaining efficient drug-enzyme interactions.[18] To that end, lipophilic ligand efficiency (LLE) was employed as a key parameter to aid in the design process and track compound progression.[19] Through this approach, tetrahydropyran **7** was discovered with the high LLE (7.9) that reflected the significant improvement in potency through the introduction of a polar oxygen heteroatom (Figure 5). The subtle decrease in polarity (HPLC Log D = 2.08) also translated to improved Cl_{int} in both rat and human (r; h Hept Cl_{int} = 70; 6 mL/min) and a large decrease in unbound in vivo rat clearance. This improved approach focused on physicochemical property considerations to simultaneously address off-target liabilities as well as refine key parameters central to drive down dose.

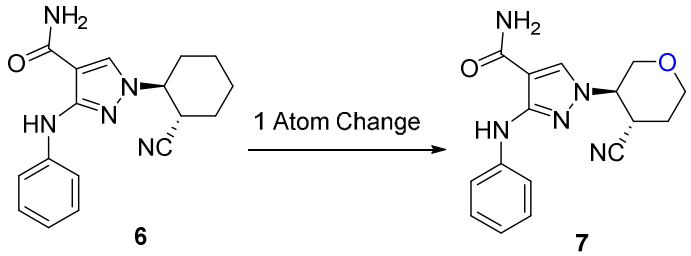

JAK1 IC_{50} (nM)	**3**	**0.4**
LBE	**0.50**	**0.56**

LLE	**5.5**	**7.9**
HPLC Log D pH 7.0	**2.66**	**2.08**
MK499 IC_{50} (nM)	**>60000**	**>60000**
Rat Cl_p (mL/min/kg)	**484**	**20**
Unbound Rat Cl (mL/min/kg	**12100**	**110**
r; h Hept Cl_{int} (mL/min/kg)	**160; 25**	**70; 6**

Figure 5. Minimal pharmacophore has high LBE and LLE

Tetrahydropyran pyrazole analogs can efficiently be synthesized in a few short steps (Scheme 1). Tetrahydro-2H-pyran-4-one (**8**) was converted to carbonitrile (**9**) by first forming the cyanohydrin with TMS-CN and TMS-OTf followed by subsequent treatment of the cyanohydrin with $POCl_3$ and elimination. Conjugate addition with pyrazole carboxamides induced by DBU afforded racemate **10**, which was separated by chiral SFC to afford enantiomerically pure **10** in 14% overall yield. With enantiomerically pure intermediate **10** in hand, Buchwald coupling with various halogenated arenes using $Pd_2(dba)_3$ and *t*-Bu X-Phos smoothly and selectively arylated the 3-amino pyrazole nitrogen.[20]

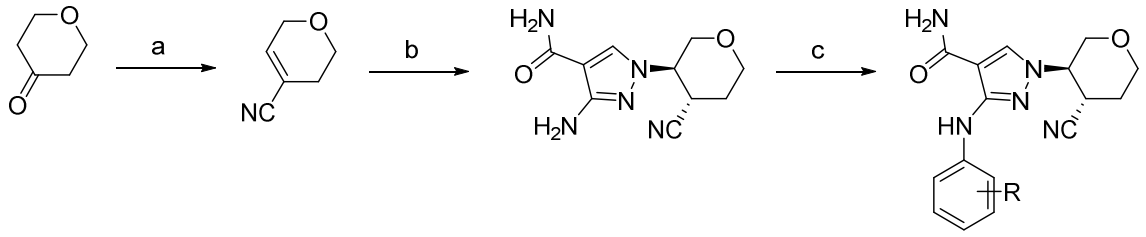

8 **9** **10** **11**

Scheme 1. Synthesis of tetrahydropyran pyrazole analogs: a) i) TMS-CN, TMS-OTf, 0 °C ii) $POCl_3$,

pyridine, 0 °C, CH_2Cl_2, 60% (two steps); b) i) 3-amino-4-pyrazole carboxamide, DBU, 70 °C, EtOH ii) chiral SFC separation of active enantiomer 14% (two steps); c) *t*-Bu XPhos, KOAc, $Pd_2(dba)_3$, 60 °C, iPrOH, 30-80%. Trimethylsilyl cyanide (TMS-CN), Trimethyl silyl trifluoromethansulfonate (TMS-OTf), Phosphoryl chloride ($POCl_3$), 1,8-Diazabicycloundec-7-ene (DBU), 2-Di-*tert*-butylphosphino-2',4',6'-triisoporopylbiphenyl (*t*-Bu XPhos).

To confirm that the new chemotype was indeed a superior series, the analogs in the tetrahydropyran chemotype (**11**) were compared to those in the earlier cylohexylamine chemotype (**12**) using a pie chart visualization analysis (Figure 6).[21] Consistent with the comparison in Figure 5, the tetrahydropyran chemotype generated a higher percentage of analogs with LLE >0.5 (87.7%) compared to the cyclohexylamine chemotype (14.5%). The increase in LLE translated to an enrichment of tetrahydropyran analogs with a cleaner hERG profile (79% with MK499 IC_{50} > 20,000 nM vs. 41% cyclohexylamine series) and increased metabolic stability (64% with Cl_{int} <20 mL/min/kg vs. 32% in the cyclohexylamine series). Bioavailability did not improve between the two series. Taken together, these analyses highlighted the enrichment of overall compound quality toward our goals of reduced hERG liability and lower projected human dose. With an efficient template in hand, we next undertook a systematic exploration of the solvent exposed aromatic ring to further optimize on LLE and understand its impact on the PK parameters, specifically rat and human Cl_{int}, bioavailability in rat, and FASSIF solubility.

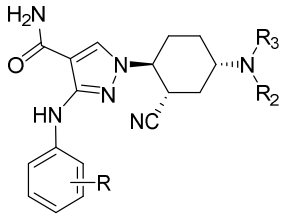

12
Cyclohexylamine Chemotype

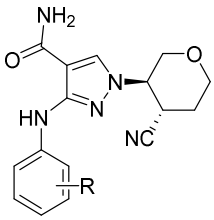

11
Tetrahydropyran Chemotype

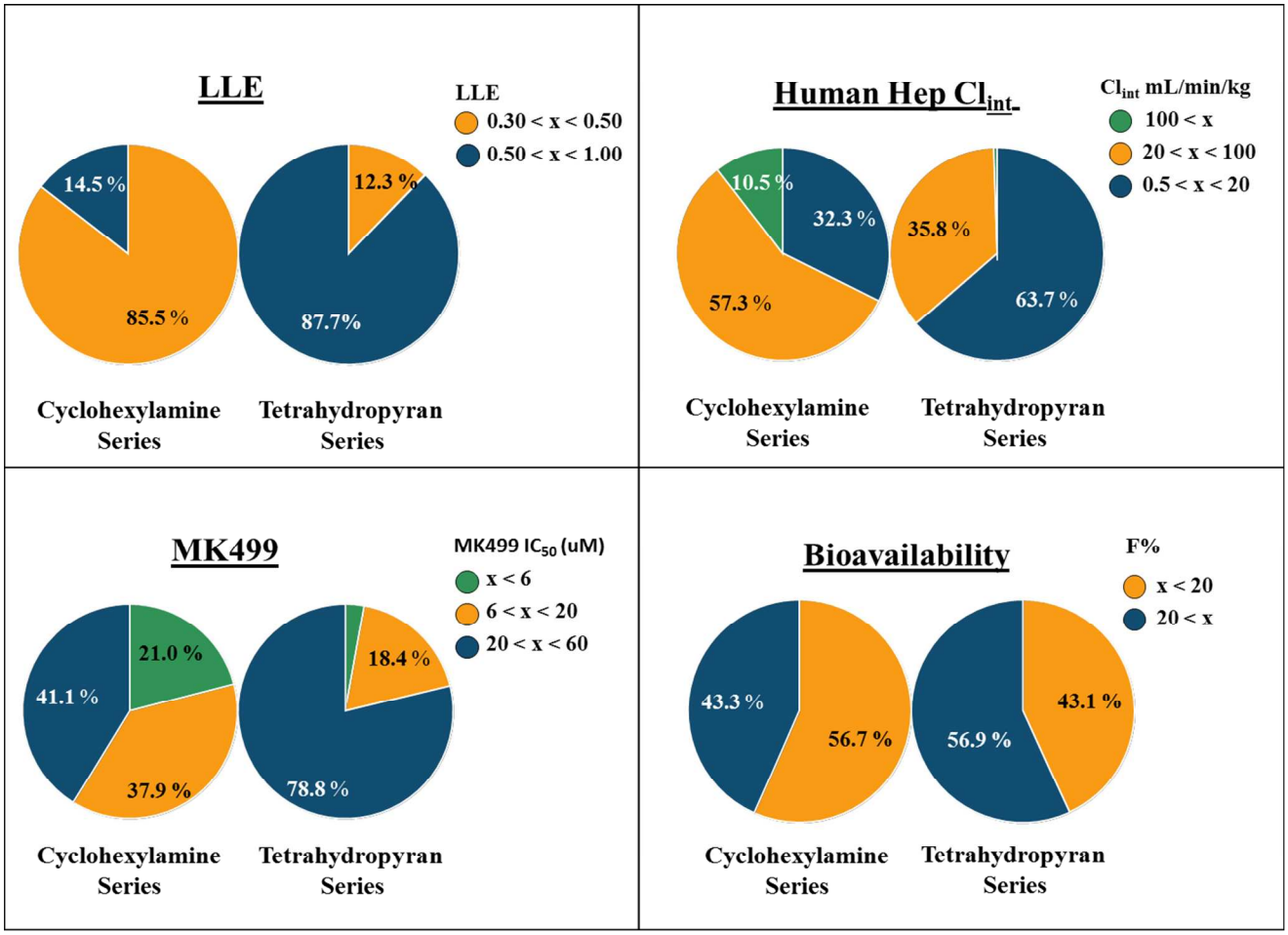

Figure 6. Binned analysis comparing LLE, MK499 IC_{50} distribution, human hepatocytes Cl_{int}, and F% between tetrahydropyran and cyclohexylamine chemotypes. Filter settings: JAK1 Enzyme IC_{50} <100 nM, Cell IL6 IC_{50} <1000 nM, 897 samples for LLE and MK499, 350 samples for human hepatocytes Cl_{int}, 88 samples for F%.

From the data shown in Table 1, lipophilic substituents on the aromatic ring such as compounds **14, 15, 16,** and **17** possessed good LLE and acceptable bioavailability; however, the increase in lipophilicity was associated with lower FASSIF solubility and higher rat and human intrinsic clearance. On the other hand, polar substituents containing heteroatoms (**18, 19, 20, 21)** generally improved rat and human intrinsic clearance (**19** r; h Hept Cl_{int} = 4.8; 2.5 mL/min/kg, **20** r; h Hept Cl_{int} = 5; 1.5 mL/min/kg, and **21** r; h Cl_{int} = <40; <20 mL/min/kg). Optimizing clearance by reducing lipophilicity was consistent with established

medicinal chemistry strategies.[22] Additionally, the added heteroatom polarity contributed to the increased FASSIF solubility as demonstrated by compound **20** (FASSIF = 159 uM). Despite the benefits of increased polarity in improving intrinsic clearance and solubility, the significant lower Log D and polarity negatively impacted the rat bioavailability with compounds **18**, **19, 20**, and **21** showing F% <20. Ultimately, optimizing for PK properties proved to be a significant challenge since the desired physicochemical profile for low Cl_{int} and high F% did not align.

To overcome the PK obstacle, we visualized the issue by plotting the impact of HPLC Log D and bioavailability and hCl_{int}. Figure 7 highlights the challenge of balancing the conflicting relationship of lipophilicity and polarity. As HPLC Log D increased, the frequency of compounds with F% >20 increased at the expense of compounds with hCl_{int} <20 mL/min/kg. The plot also revealed that HPLC Log D 1.50-2.50 was the optimal range for both bioavailability and hCl_{int} properties. This analysis provided a targeted range to enable design of inhibitors in the desired property space.

Table 1: Structure activity relationship of tetrahydropyrans

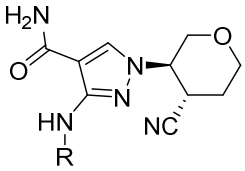

11

Compound	R	JAK1; 2; 3; TYK2 IC_{50}(nM) [a]	Ratio JAK 2/ 1	Cell IL6;EPO IP (nM)[b]	LLE[c]	MK499 IC_{50}(nM)[d]	Hepatocyte Cl_{int}mL/min/ kg (rat;human)[g]	F (%)[f]	HPLC LogD pH7.0[g]	FASSIF(uM)
13	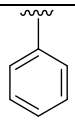	0.4; 3; 361; 2.9	8X	33; 209 (6X)	7.90	>60000	70; 6	79	2.08	18

14	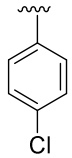	**0.13; 1.5; 256; 2**	**12X**	**14; 140 (10X)**	**7.72**	**40000**	**9; 85**	**71**	**2.57**	**39**
15	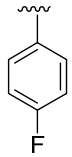	**0.3; 2; 304; 1.8**	**7X**	**31; 334 (11X)**	**7.82**	**40000**	**<40; <20**	**40**	**2.18**	**42**
16	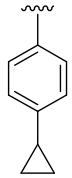	**0.5; 1.9; 280; 3.9**	**4X**	**37; 200 (5X)**	**6.98**	**35000**	**262; 41**	**NA**	**2.58**	**NA**
17	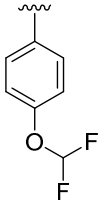	**0.1; 0.8; 196; 0.7**	**11X**	**5; 54 (11X)**	**7.69**	**25000**	**59; 28**	**42**	**2.27**	**NA**
18	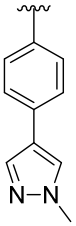	**0.02; 0.5; 91; 0.2**	**23X**	**6; 39 (7X)**	**8.03**	**>60000**	**55; <20**	**18**	**1.48**	**42**
19	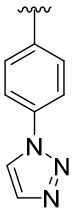	**0.06; 0.7; 116; 0.5**	**11X**	**23; 254 (11X)**	**8.96**	**13200**	**4.8; 2.5**	**3**	**1.00**	**96**
20	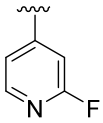	**0.24; 2.8; 511; 3**	**10X**	**42; 414 (10X)**	**8.68**	**>60000**	**5; 1.5**	**19**	**1.18**	**159**

21	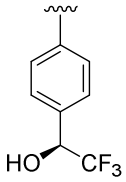	**0.05; 0.47; 100; 0.4**	**9X**	**14; 48 (3X)**	**8.37**	**>60000**	**<40; <20**	**9**	**1.93**	**NA**
22	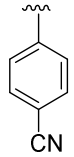	**0.15; 1.2; 230; 1.2**	**8X**	**13; 89 (7X)**	**8.44**	**40000**	**6; 3**	**47**	**1.77**	**130**

[a]Values in this table are determined by the HTRF assay and are the means from at least n = 2 experiments. [b]Values in this table are determined by GeneBLAzer assay and are the means from at least n = 2 experiments. [c]Values are calculated from pIC_{50} – ALogP98. [d]hERG binding assay, ref 13. [f]Dose; rat iv 0.5 mg/kg as a solution in PEG400:H_2O (60:40 (v/v)), po: 1 mg/kg as a solution in PEG400:H_2O (60:40 (v/v)). [g]See supporting information. NA = not available.

With a target physicochemical range in mind, we turned our attention to identifying SAR that fit within the desired HPLC Log D range. The introduction of a nitrile is a useful functional group that embodies polar features without significantly reducing Log D.[23] To explore this concept, **22** was prepared and exhibited a balanced HPLC Log D (1.77) without compromising LLE (8). This balanced profile translated to a low r; h intrinsic clearance (r; h Hept Cl_{int} = 6; 3 mL/min/kg) with a desired aqueous solubility (FASSIF = 130 uM) without compromising the bioavailability (F% = 47).

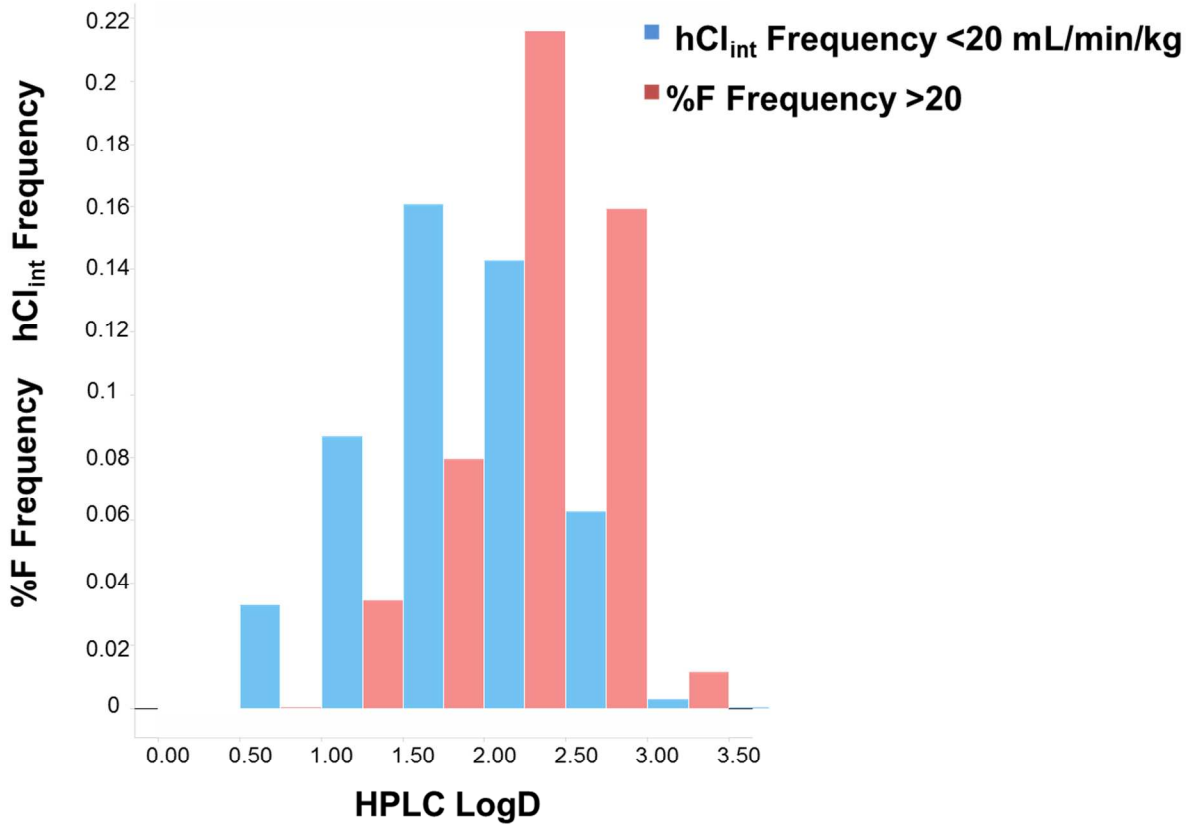

Figure 7. Analysis of %F and Cl_{int} frequency plotted against HPLC Log D. HPLC Log D between 1.50-2.50 is the optimal range. Filter settings: JAK1 Enzyme IC_{50} <100 nM, Cell IL6 IC_{50} <1000 nM.

The favorable profile of **22** warranted further animal and human ADME data as well as human whole blood potency to inform on human dose prediction (Table 2).[9] Gratifyingly, in vitro Cl_{int} correlated well with the in vivo unbound clearance (Cl_u) across species, allowing for confidence in human in vitro in vivo extrapolation (IVIVE). Allometric scaling and translatable exposure to higher order species combined with the human whole blood potency (HWB IL7 IC_{50} = 220 nM) informed to project the predicted human dose for **22** at 15 mg QD with an excellent D_0 = 2. The excellent dose and dose number for **22** validated our approach of optimizing on intrinsic potency, Cl_{int}, solubility, and bioavailability in order to identify a low dose lead molecule.

Table 2. Pharmacokinetic parameters of compounds 22 and 28 in preclinical species

	Rat[a]		Dog[b]		Cyno[c]		Predicted Human[d]	
	22	**28**	**22**	**28**	**22**	**28**	**22**	**28**
Cl_p (mL/min/kg)	19	21	12	14	2.4	19	0.9	0.6
Hept Cl_{int}[e]	6	35	20	122	6	36	3	6
PPB %	81	94	82	NA	79	96.7	78	97.8
Cl unbound (mL/min/kg)	100	350	67	NA	12	581	4	27
Vd_{ss} (L/kg)	2.6	2.7	2.7	1.2	1	2.4	2.3	1
$t_{1/2}$ (hr)	1.4	1.6	2.6	1.1	5.6	2.8	30	20
F (%)	47	47	51	29	18	32	72	56
Human Whole[e] Blood (nM)							220	1760
Dose (QD) (mg)[d]							15	81
Dose Number[f]							2	25

[a]Dose; rat iv 0.5 mg/kg as a solution in PEG400:H_2O (60:40 (v/v)), po: 1 mg/kg as a solution in PEG400:H_2O (60:40 (v/v)). [b]Dose dog iv 0.25 mg/kg as a solution in DMSO:PEG400:water(20:60:20), cyno PO 0.5 mg/kg as a solution in PEG400/TWEEN80/H_2O(20:60:20) [c]Dose; cyno iv 0.25 mg/kg as a solution in DMSO:PEG400:water(20:60:20), cyno PO 0.5 mg/kg as a solution in captisol 30%. [d]See reference 9 [e]See supporting information. [f]See reference 11a.

Despite the successful approach of focusing on physicochemical properties and dose to identify **22** with favorable drug like properties, the optimization process eroded the JAK1 pathway selectivity of **22** (7-

fold), precluding further development of the molecule. During the rapid SAR screening process of the aromatic vector of the inhibitor, compound **23** with 50-fold selectivity for JAK1 over JAK2 was identified. Examining the structural uniqueness of **23**, we hypothesized that projecting into the southeast region of the aromatic ring might account for the enhanced selectivity. To further test this hypothesis and exploit this potential unique interaction, we combined the findings from Table 1 with SAR at the southwest region of the aromatic ring (Table 3). Consistent with the same strategy as in Table 1, we were mindful of optimizing for selectivity while maintaining desirable LLE in order to refine PK parameters that related to lowering dose. Using **22** as a baseline with 8-fold selectivity in enzyme activity and 7-fold in cellular activity, introduction of a meta methoxy group (**24**) enhanced the JAK2/JAK1 selectivity to 46-fold in the enzyme and 23-fold in the pathway assay. Additional changes including Cl, CN, and cyclopropyl as exemplified by **25**, **26**, **27** led to modest improvements in selectivity which suggest the unique positioning of a methoxy group was critical for selectivity. Additionally, this SAR was translatable to other promising aromatic analogs such **28**, **29**, **30**. Notably, accessing the same vector by constraining small substituents using fused rings led to even greater selectivity as demonstrated by **31**, **32**, and **33,** achieving >50-fold in enzyme and >80-fold selectivity in cell assays. Despite the exquisite selectivity from the fused ring analogs, these compounds did not possess the desired in vitro and in vivo PK properties to progress further.

The new meta substituent discovery expanded our SAR resulting in numerous highly selective compounds with desirable PK properties. Notably, the balanced properties of compound **28** with a para chloro and meta methoxy not only imparted improved JAK1 selectivity (39-fold enzyme and 25-fold cell) but also retained favorable rat Cl_u (350 mL/min/kg) with low hept hCl_{int} (6 mL/min/kg) and desirable bioavailability (F% = 47). The overall selectivity and dose parameters for **28** were superior to other analogs and consequently progressed to full PK determinations (Table 2). Evaluation of **28** in multiple species across a panel of studies revealed a good correlation between in vitro hept Cl_{int} and in vivo Cl_u, leading to a confident low human predicted total clearance of 0.6 mL/min/kg with a half-life of 20 hr and bioavailability of 56%. Furthermore, the predicted human PK properties combined with the human whole blood (IC_{50} = 1760 nM) led to the predicted human dose of 81 mg QD with a D_0 = 25.

Table 3. Structure activity relationship of tetrahydropyrans

Compound	R	JAK1; 2; 3; TYK 2 IC_{50} (nM)[a]	Ratio JAK2; JAK1	Cell IL6; EPO[b] IP (nM)[b]	LLE[c]	Rat Cl_u[d] mL/min/kg	Hepatocyte Cl_{int}mL/min kg (rat; human)[e]	F (%)[d]	HPLC Log pH 7.0[e]
23	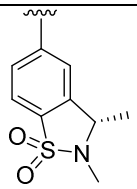	0.04; 2; 315; 1.7	50X	16; 224 (14X)	9.65	535	62; 62	NA	3.15
24	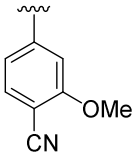	0.07; 3.2; 391; 9	46X	19; 430 (23X)	8.79	310	<40; 24	2	1.87
25	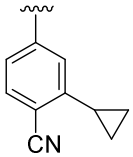	1.4; 16; >1496; 40	11X	72; 744 (10X)	7.95	NA	NA	NA	2.34
26	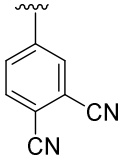	0.9; 5; 656; 11	6X	77; 1192 (15 X)	7.79	NA	NA	NA	1.99
27	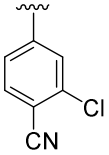	0.4; 2.7; 556; 4	7X	26; 261 (10X)	7.35	268	NA	23	2.18
28	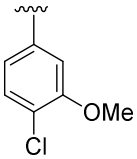	0.1; 3.9; 397; 12	39X	13; 320 (25X)	7.85	350	35; 6	47	2.34

29	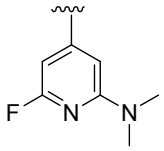	**0.18; 3.4; 701 ; 13**	**19X**	**28; 530 (19X)**	**8.11**	**522**	**9; 4**	**4**	**2.07**
30	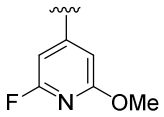	**0.4; 6; 1130; 13**	**15X**	**39; 600 (15X)**	**7.94**	**108**	**14; 2**	**49**	**1.89**
31	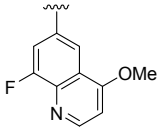	**0.19; 10; >1496; 8**	**53X**	**24; 2114 (88x)**	**7.85**	**500**	**15; 15**	**NA**	**1.40**
32	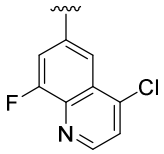	**0.24; 7; 1012; 12**	**29X**	**14; 608 (43X)**	**7.06**	**1212**	**52; 25**	**19**	**1.81**
33	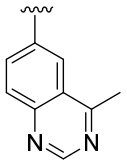	**0.16; 7; 783; 14**	**43X**	**24; 1635 (68X)**	**8.45**	**NA**	**NA**	**NA**	**1.02**

[a]Values in this table are determined by the HTRF assay and are the means from n = 2 experiments. [b]Values in this table are determined by GeneBLAzer assay and are the means from at least n = 2 experiments. [c]Values are calculated from pIC_{50} – ALogP98. [d]Dose; rat iv 0.5 mg/kg as a solution in PEG400:H_2O (60:40 (v/v)), po: 1 mg/kg as a solution in PEG400:H_2O (60:40 (v/v)). [e]See supporting information. NA = not available.

Having significantly altered the structure from starting point **2**, the off target kinase profile of **28** was assessed in a broad kinase panel consisting of 265 kinases.[24] Kinase selectivity of **2**, **22**, and **28** is depicted using a radar plot where the distance from the center is proportional to the fold selectivity over JAK1 in log_{10} units. As shown in Figure 8, **28** was more selective and differentiated from **2** since its curve

lies outside that of **2**. In addition to the radar plot, several additional metrics were also used to analyze kinase selectivity from different perspectives. While the percentage of kinases with at least 100-fold selectivity is a common metric used to understand selectivity it can be misleading if the few kinases under 100-fold are equally potent or more potent than the target kinase. Alternatively, the partition index method can be used to quantify the fraction of the inhibitor that would be bound to the target of interest at thermodynamic equilibrium, with values closer to one indicating that the ligand is highly selective and binds only to the desired target.[25] Lead compound **28** is a highly selective for JAK1 inhibitor demonstrating greater than 100-fold selectivity over 99% of the 265 kinases tested with a partition index of 0.94 (Figure 8).

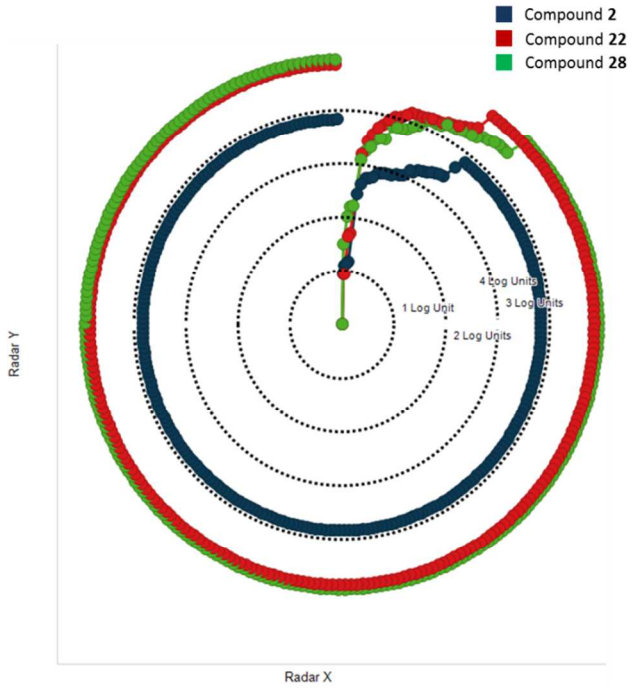

Compounds	% Kinases >100 X Over JAK1	Partition Index
2	98	0.72
22	98	0.78
28	99	0.94

Figure 8. Analysis of kinase selectivity profile of compounds **2**, **22**, **28** against 265 kinases using a radar plot, percent of kinases at least100-fold selectivity over JAK1 and partition index.

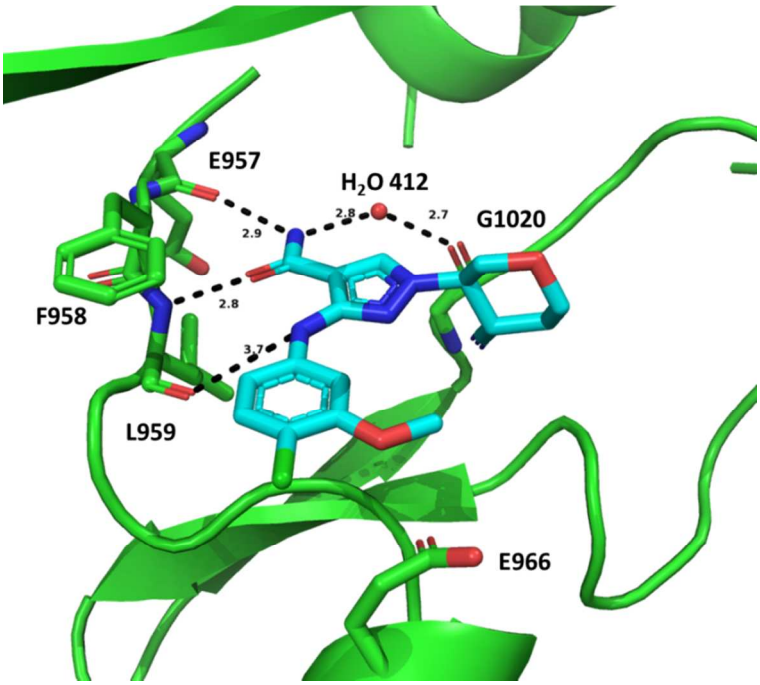

Figure 9. Co-crystal structure of **28** in JAK1 kinase domain showing ligand protein interactions (PDB 5WO4)

In order to gain greater clarity on the protein-ligand molecular interactions and the nature of the JAK isoform selectivity, crystallographic studies of **28** were examined. Figure 9 shows compound **28** binding to the active site of the JAK1 kinase domain.[26] The primary amide anchors the ligand by making hydrogen bonds to the backbone carbonyl oxygen of Glu957 and the backbone amide NH of Leu959 in the hinge region of the kinase. Additionally, the primary amide is involved in a water molecule (H_2O-412 in PDB 5WO4) mediated hydrogen bond interaction with the backbone carbonyl oxygen atom of Gly1020 in the back pocket. The para position of the aniline projects out to solvent, consistent with the flexible SAR

observed in this region of the molecule. Furthermore, the cyano substituted tetrahydropyran ring forces an increased dihedral angle resulting in hydrophobic packing in two deep pockets. The tetrahydropyran oxygen is buried under the glycine rich loop (omitted for clarity in Figure 9); however, this interaction is poorly understood because simple van der Waals interactions do not satisfyingly explain the 10-fold decrease in potency when lipophilic cyclohexane is substituted for the tetrahydropyran. Furthermore, the twisted conformation of the tetrahydropyran projects the nitrile group into a small hydrophobic back-pocket created by Leu1010 and Gly1020 unique to JAK family kinases. The combination of these unique interactions in conjunction with the conserved water molecule H_2O-412 mediated hydrogen bond confers the excellent JAK family kinase selectivity.

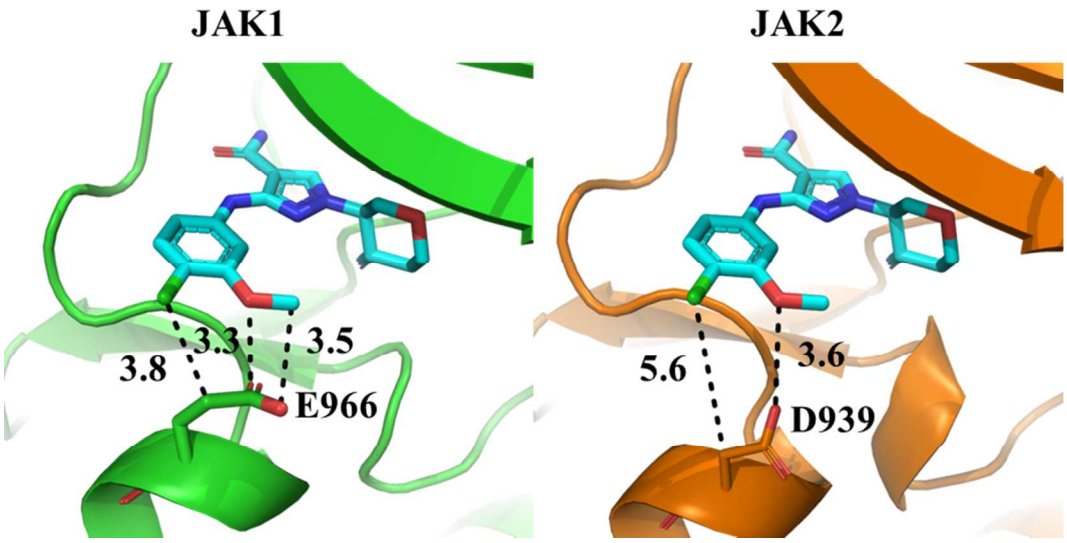

Figure 10. Comparison of **28** contacts with residues Glu966 in JAK1 and Asp939 in JAK2. In the crystal structure of **28** bound to JAK1, the dashed lines correspond to van der Waals contacts between the ligand and Glu966 identified with the ViewContacts software. No van der Waals interactions were identified when **28** was modeled into the active site of JAK2 (PDB 3LPB).

To determine the nature of the JAK isoform selectivity, comparison of the x-ray crystal structures of **28** bound to human JAK1 and overlaid on a JAK2 crystal structure revealed a unique 3-methoxy group

interaction with a single amino acid difference between JAK1 and JAK2.[27] In particular, the 3-methoxy group interacts with the longer side residue Glu966 in JAK1 through van der Waals interactions, whereas in JAK2 the equivalent residue (Asp939) is positioned further away from any direct interaction (Figure 10).[28] Interestingly, this finding is consistent with the observations of Kim *et al* and Zak *et* al, which led to the elegant designs of selective JAK1 inhibitors.[6d,f] Overall, our findings along with others suggest that exploiting the Glu966 residue in JAK1 is a general and consistent strategy to optimize for JAK1 selectivity over JAK2.

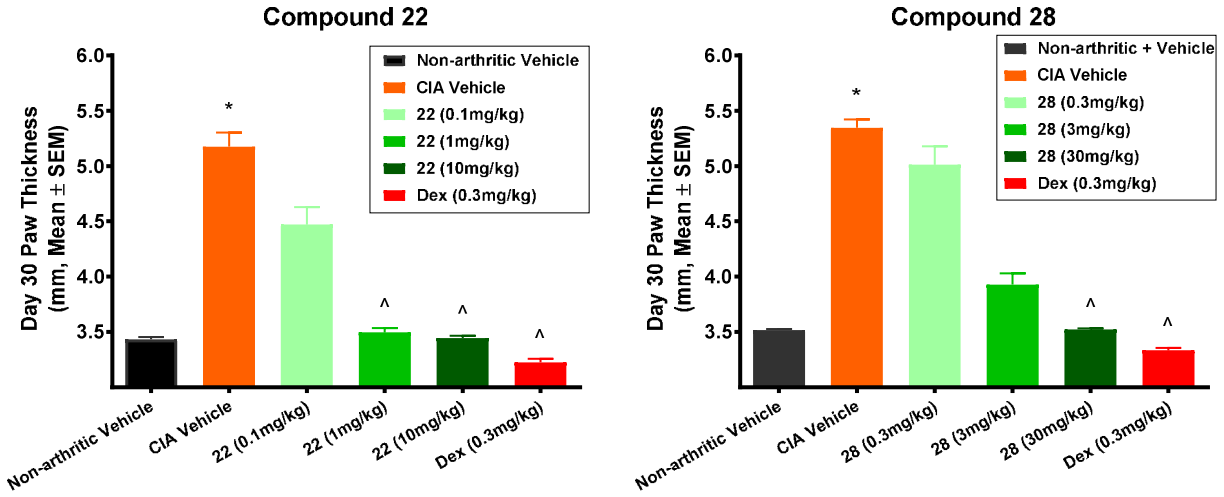

Figure 11. Compound **22** dosed PO BID at 0.1, 1, 10 mg/kg and **28** PO BID at 0.3, 3, 10, 30 mg/kg were efficacious in reducing paw swelling in a 30 day rat CIA model. Dexamethasone was included as a positive control. .*$p < 0.005$, statistically different from non-arthritic controls, ^$p < 0.005$, statistically different from CIA vehicle group.

On the basis of the favorable lead compound profile, in vivo properties, and kinase selectivity, compounds **22** and **28** were studied in a rat collagen induced arthritis model (CIA)[29] using a therapeutic dosing paradigm (Figure 11).[30] Rats were immunized and boosted with collagen intradermally at the base of the tail on days one and seven. Animals were stratified into treatment groups with comparable levels of paw

inflammation on day 16 and treatment with compounds **22** and **28** (p.o. BID) and dexamethasone (p.o QD) was initiated on day 17. Both compounds exhibited dose dependent inhibition of inflammation. The maximum attenuation of paw swelling with compounds **22** and **28** was achieved with 10 and 30 mg/kg respectively, which was comparable to dexamethasone treated CIA non arthritic control groups. Compound **28** demonstrated that selectively inhibiting the JAK1 pathway is sufficient to drive efficacy in a preclinical inflammation model and suggests that JAK1 selective compounds may offer an advantage by offsetting the potential anemia side effects of inhibiting JAK2.

Conclusion

In conclusion, while the lead compound **2** in the cyclohexylamine series served as a useful tool to probe the effects of JAK1 selectivity, further progression of that chemotype was challenging due to hERG activity and high predicted human dose. To address these issues, we attempted to optimize and differentiate analogs in that series based on the parameters associated with predicted human dose including intrinsic potency, Cl_{int}, bioavailability, and solubility. Multiparameter optimization on compound **2** proved to be a difficult endeavor due to opposing SAR between decreasing hERG and PK parameters. A shift in strategy toward a new core with the tetrahydropyran chemotype followed by LLE guided optimization produced an enriched cohort of analogs with reduced hERG signal and improved PK parameters. In conjunction with these advances, structural chemistry information provided key insights in guiding modifications to improve JAK1 selectivity, in particular revealing a key amino acid difference between JAK1 and JAK2. By exploiting selectivity advancements in combination with the improved tetrahydropyran core, a significant enrichment of JAK1 selective compounds with the desired drug like properties and low predicted human dose were synthesized. These efforts culminated in the discovery of JAK1 selective compound **28,** which has an excellent predicted human dose projection of 81 mg QD and is highly active in our CIA inflammation model. Furthermore, the pathway selectivity of **28** allowed for further pharmacological investigation into delineating an improved therapeutic index with a JAK1 selective compound. This data will be reported in a future communication.

Experimental Section

General experimental methods. Commercial reagents were obtained from reputable suppliers and used as received. All solvents were purchased in septum–sealed bottles stored under an inert atmosphere. All reactions were sealed with septa through which an argon atmosphere was introduced unless otherwise noted. Liquid reagents and solvents were transferred under a positive pressure of nitrogen via syringe. Reactions were conducted in microwave vials or round bottomed flasks containing Teflon–coated magnetic stir bars. Microwave reactions were performed with a Biotage Initiator Series Microwave (fixed hold time setting; reaction temperatures monitored by the internal infrared sensor). Reactions were monitored by thin layer chromatography (TLC) on pre–coated TLC glass plates (silica gel 60 F254, 250 μm thickness) or by LC/MS (30 mm x 2 mm 2 μm column + guard; 2 μL injection; 3% to 98% MeCN/water + 0.05% TFA gradient over 2.3 minutes; 0.9 mL/min flow; ESI; positive ion mode; UV detection at 254 nm). Visualization of the developed TLC chromatogram was performed by fluorescence quenching. Flash chromatography was performed on an automated purification system using pre–packed silica gel columns. ^{1}H NMR spectra were recorded on either a 500 or a 600 MHz Varian spectrometer; chemical shifts (δ) are reported relative to residual proton solvent signals. Data for NMR spectra are reported as follows: chemical shift (δ ppm), multiplicity (s = singlet, brs = broad singlet, d = doublet, t = triplet, q = quartet, dd = doublet of doublets, td = triplet of doublets, m = multiplet), coupling constant (Hz), integration. All final compounds possess a purity of at least 95% as determined by ^{1}H NMR, LCMS, HRMS.

3,6-dihydro-2H-pyran-4-carbonitrile (9)

To the solution of trimethylsilyl cyanide (105 g, 1080 mmol) in DCM (370 mL) were added tetrahydro-4H-pyran-4-one (90 g, 900 mmol) and trimethylsilyl triflate (6 g, 27 mmol) at 0 ^{o}C. The resulting mixture was stirred at 0 ^{o}C for 1 hour before the addition of pyridine (1120 mL) and phosphoryl chloride (413 g, 2700 mmol). The mixture was refluxed for 12 hours, and then poured into the mixture of 2N hydrochloric acid

aqueous solutions (1.5 L), and extracted with EtOAc (3*2 L). All the organic solutions were washed with brine (2*1000 mL), dried over sodium sulfate, filtered and concentrated under vacuum. The crude residue was purified by column chromatography (eluted with PE / EtOAc = 10 / 1) to give 3,6-dihydro-2H-pyran-4-carbonitrile (59 g, 60.1 %) as a yellow oil. ^{1}H NMR (300 MHz, $CDCl_3$) δ 6.62 – 6.59 (m, 1H), 4.29 – 4.21 (m, 2H), 3.78 (t, *J* = 5.4 Hz, 2H), 2.34 – 2.30 (m, 2H).

3-amino-1-((3R,4S)-4-cyanotetrahydro-2H-pyran-3-yl)-1H-pyrazole-4-carboxamide (10)

The solution of 3-amino-1H-pyrazole-4-carboxamide (85 g, 671 mmol), 3,6-dihydro-2H-pyran-4-carbonitrile (205 g, 1.88 mol) and DBU (234 g, 1.54 mol) in ethanol (850 mL) was stirred at 70 ^{o}C overnight under nitrogen and then concentrated under vacuum. The crude residue was purified by silica gel flash column chromatography (eluted with DCM / Methanol = 30 / 1) to yield racemic compound 10 (47 g, 29.8 %) as a yellow solid. The chiral separation of 380 g of the racemic compound was accomplished by dissolving in ACN/MeOH (1:1) to a concentration of 25 mg/mL. Injections of 16 mL were made on a Thar 350 preparative SFC (Column: ChiralPak IC-10 μM, 300x50 mm; Mobile phase: 45% 2-propanol, 55% CO2; Flow rate: 220 mL/min; Column temperature: 38 °C). After separation, the fractions were dried by rotary evaporation to give 3-amino-1-((3S,4R)-4-cyanotetrahydro-2H-pyran-3-yl)-1H-pyrazole-4-carboxamide (174 g, 48.8 %, 99.6 % ee) from the first (faster eluting) peak and 3-amino-1-((3R,4S)-4-cyanotetrahydro-2H-pyran-3-yl)-1H-pyrazole-4-carboxamide (181 g, 47.6%, 99.6% ee) from the second (slower eluting) peak. The absolute configuration of stereochemistry was determined from X-ray crystallography of compound 28 with JAK1 protein. The second (slower eluting) peak was carried on to to generate SAR. ^{1}H NMR (500 MHz, DMSO-d_6) δ 8.03 (s, 1H), 7.36 (brs, 1H), 6.80 (brs, 1H), 5.36 (s, 2H), 4.86-4.31 (td, *J* = 10.5, 4.5 Hz, 1H), 3.91-3.88 (dd, *J* = 11.5, 4.5 Hz 1H), 3.86 – 3.83 (m, 1H), 3.53-3.50 (m, 2H), 3.39-3.33 (td, *J* = 11.5, 2 Hz, 1H), 2.10-2.07 (m, 1H), 1.95-1.87 (m, 1H). ^{13}C NMR (500 MHz, DMSO-d_6): δ 166.3, 157.2, 131.6, 120.2, 101.2, 69.8, 65.8, 57.8, 31.9, 28.5. LRMS (ESI) calc'd for $C_{10}H_{14}N_5O_2$ $[M+H]^+$: 236, Found: 236.

1-((3R,4S)-4-cyanotetrahydro-2H-pyran-3-yl)-3-(phenylamino)-1H-pyrazole-4-carboxamide (**13**). Prepared following similar procedure described for **28** in 57% yield. LRMS (ESI) calcd for ($C_{16}H_{17}N_5O_2$) $[M + H]^+$ 312.1, found 312.1. HRMS: calcd for ($C_{16}H_{17}N_5O_2$) $[M + H]^+$ 312.1460, found 312.1451; difference 2.9 ppm. ^{1}H NMR (500 MHz, CD_3OD) δ 8.17 (s, 1H), 7.51-7.50 (d, *J* = 8.7 Hz, 2H). 7.26-7.23 (t, *J* = 16.1, 8.1 Hz, 2H), 6.87-6.84 (t, *J* = 14.5, 7.4 Hz, 1H), 4.44-4.39 (m, 1H), 4.12-4.08 (m, 1H), 4.01-3.97 (m, 1H), 3.90-3.86 (m, 1H), 3.72-3.66 (m, 1H), 3.60-3.55 (m, 1H), 2.23-2.18 (m, 1H), 2.09-2.01 (m, 1H). ^{13}C NMR (500 MHz, DMSO-d_6): δ 166.4, 153.05, 141.7, 131.6, 129.4 (2C), 120.23, 120.03, 116.4 (2C), 101.3, 69.4, 65.8, 58.0, 31.9, 28.4. $[\alpha]_D^{20}$ +145 (*c* 0.83, MeOH/DMSO 2:1).

3-((4-chlorophenyl)amino)-1-((3R,4S)-4-cyanotetrahydro-2H-pyran-3-yl)-1H-pyrazole-4-carboxamide (**14**). Prepared following similar procedure described for **28** in 45% yield. LRMS (ESI) calcd for ($C_{16}H_{16}ClN_5O_2$) $[M + H]^+$ 346.1, found 346.1. HRMS: calcd for ($C_{16}H_{16}ClN_5O_2$) $[M + H]^+$ 346.1071, found 346.1063; difference 2.3 ppm. ^{1}H NMR (500 MHz, $CDCl_3$) δ 8.83 (s, 1H), 7.77 (s, 1H), 7.47-7.45 (d, *J* = 8.7 Hz, 2H), 7.25-7.23 (d, *J* = 9 Hz, 2H), 5.48 (brs, 2H), 4.25-4.21 (m, 1H), 4.19-4.15 (m, 1H), 4.06-4.02 (m, 2H), 3.68-3.64 (m, 1H), 3.60-3.56 (m, 1H), 2.17-2.14 (m, 1H), 2.07-1.99 (m, 1H).

1-((3R,4S)-4-cyanotetrahydro-2H-pyran-3-yl)-3-((4-fluorophenyl)amino)-1H-pyrazole-4-carboxamide (**15**). Prepared following similar procedure described for **28** in 40% yield. LRMS (ESI) calcd for ($C_{16}H_{16}FN_5O_2$) $[M + H]^+$ 330.1, found 330.1. ^{1}H NMR (600 MHz, DMSO-d_6) δ 9.10 (s, 1H), 8.25 (s, 1H), 7.67 (brs, 1H), 7.52-7.48 (m, 2H), 7.13 (brs, 1H), 7.06-7.03 (t, *J* = 8.9 Hz, 2H), 4.54-4.49 (m, 1H), 3.99-3.96 (m, 1H), 3.88-3.86 (m, 1H), 3.66-3.61 (m, 2H), 3.47-3.42 (m, 1H), 2.12-2.09 (m, 1H), 1.97-1.91 (m, 1H).

1-((3R,4S)-4-cyanotetrahydro-2H-pyran-3-yl)-3-((3-cyclopropylphenyl)amino)-1H-pyrazole-4-carboxamide (**16**).Prepared following similar procedure described for **28** in 17% yield. LRMS (ESI) calcd for ($C_{19}H_{21}N_5O_2$) $[M + H]^+$ 352.2, found 352.2. HRMS: calcd for ($C_{19}H_{21}N_5O_2$) $[M + H]^+$ 352.1773, found

352.1767; difference 1.7 ppm. ^{1}H NMR (500 MHz, DMSO-d_6) δ9.08 (s, 1H), 8.28 (s, 1H), 7.71 (brs, 1H), 7.33-7.32 (d, *J* = 7.8 Hz, 1H), 7.16 (brs, 1H), 7.13-7.10 (t, *J* = 7.8 Hz, 2H), 6.57-6.56 (d, *J* = 7.3 Hz, 1H), 4.57-4.53 (m, 1H), 4.05-4.02 (m, 1H), 3.92-3.90 (m, 1H), 3.68-3.61 (m, 2H), 3.48-3.43 (m, 1H), 2.17-2.15 (m, 1H), 2.01-1.95 (m, 1H), 1.91-1.86 (m, 1H), 0.93-0.92 (d, *J* = 7.44 Hz, 2H), 0.67 (brs, 2H).

1-((3R,4S)-4-cyanotetrahydro-2H-pyran-3-yl)-3-((4-(difluoromethoxy)phenyl)amino)-1H-pyrazole-4-carboxamide (**17**). Prepared following similar procedure described for **28** in 17% yield. LRMS (ESI) calcd for ($C_{17}H_{17}F_2N_5O_3$) [M + H]$^+$ 378.2, found 378.2. HRMS: calcd for ($C_{17}H_{17}F_2N_5O_3$) [M + H]$^+$ 378.1377, found 378.1379; difference -0.5 ppm. ^{1}H NMR (500 MHz, DMSO-d_6) δ 9.16 (s, 1H), 8.27 (s, 1H), 7.72 (brs, 1H), 7.56-7.54 (d, *J* = 7.8 Hz, 2H), 7.18 (brs, 1H), 7.22-6.92 (dd, *J* = 73, 6.8 Hz, 1H), 7.07-7.06 (d, *J* = 6.8 Hz, 2H), 4.57-4.52 (m, 1H), 4.02-3.99 (m, 1H), 3.90-3.88 (m, 1H), 3.69-3.63 (m, 2H), 3.49-3.44 (m, 1H), 2.14-2.12 (m, 1H), 2.00-1.92 (m, 1H).

1-((3R,4S)-4-cyanotetrahydro-2H-pyran-3-yl)-3-((4-(1-methyl-1H-pyrazol-4-yl)phenyl)amino)-1H-pyrazole-4-carboxamide (**18**). Prepared following similar procedure described for **28** in 10% yield. LRMS (ESI) calcd for ($C_{20}H_{21}N_7O_2$) [M + H]$^+$ 392.2, found 392.2. ^{1}H NMR (500 MHz, DMSO-d_6) δ 9.55 (s, 1H), 8.94-8.93 (d, *J* = 2.6 Hz, 1H), 8.68-8.67 (d, *J* = 2.3 Hz, 1H), 8.30 (s, 1H), 7.95-7.93 (d, *J* = 8.8 Hz, 1H), 7.92-7.91 (d, *J* = 1.9 Hz, 1H), 7.76 (brs, 1H), 7.55-7.52 (dd, *J* = 8.7, 2.1 Hz, 1H), 7.26 (brs, 1H), 4.46-4.41 (m, 1H), 3.44 (s, 3H), 2.19-2.17 (m, 1H), 2.03-1.99 (m, 1H), 1.94-1.86 (m, 1H), 1.83-1.79 (m, 1H), 1.76-1.71 (m, 2H), 1.48-1.38 (m, 2H).

3-((4-(1H-1,2,3-triazol-1-yl)phenyl)amino)-1-((3R,4S)-4-cyanotetrahydro-2H-pyran-3-yl)-1H-pyrazole-4-carboxamide (**19**). Prepared following similar procedure described for **28** in 9% yield. LRMS (ESI) calcd for ($C_{18}H_{18}N_8O_2$) [M + H]$^+$ 379.1, found 379.1. ^{1}H NMR (500 MHz, DMSO-d_6) δ 9.39 (s, 1H), 8.70 (d, *J* = 0.93 Hz, 1H), 8.31 (s, 1H), 7.91 (d, *J* = 0.93 Hz, 1H), 7.76 (brs, 1H), 7.77-7.75 (d, *J* = 9.1 Hz, 2H), 7.73-7.71 (d, *J* = 9.1 Hz, 2H), 7.24 (brs, 1H), 4.61-4.56 (m, 1H), 4.05-4.02 (m, 1H), 3.93-3.89 (m, 1H),

3.73-3.66 (m, 2H), 3.50-3.46 (m, 1H), 2.16-2.14 (m, 1H), 2.02-1.94 (m, 1H).

1-((3R,4S)-4-cyanotetrahydro-2H-pyran-3-yl)-3-((2-fluoropyridin-4-yl)amino)-1H-pyrazole-4-carboxamide (**20**). Prepared following similar procedure described for **28** in 51% yield. LRMS (ESI) calcd for ($C_{15}H_{16}FN_6O_2$) $[M + H]^+$ 331, found 331. HRMS: calcd for ($C_{15}H_{16}FN_6O_2$) $[M + H]^+$ 331.1319, found 331.1307; difference 3.6 ppm. ^{1}H NMR (500 MHz, DMSO-d_6) δ 9.74 (s, 1H), 8.35 (s, 1H), 7.93 (d, *J* = 6 Hz, 1H), 7.84 (s, 1H), 7.33 (m, 3H), .4.65 - 4.60 (td, *J* = 10.5, 4.5 Hz, 1H), 4.04-4.00 (dd, *J* = 11.5,, 4.5, 1H), 3.90 - 3.88 (m, 1H), 3.73- 3.63 (m, 2H), 3.51-3.46 (td, *J* = 11.5, 2 Hz, 1H), 2.15-2,12 (m, 1H), 2.00-1.93 (m, 1H).

1-((3R,4S)-4-cyanotetrahydro-2H-pyran-3-yl)-3-((4-(2,2,2-trifluoro-1-hydroxyethyl)phenyl)amino)-1H-pyrazole-4-carboxamide (**21**). Prepared following similar procedure described for **28** in 49% yield. LRMS (ESI) calcd for ($C_{18}H_{18}F_3N_5O_3$) $[M + H]^+$ 410.1, found 410.1. ^{1}H NMR (500 MHz, DMSO-d_6) δ 9.24 (s, 1H), 8.30 (s, 1H), 7.74 (brs, 1H), 7.55-7.54 (d, *J* = 7.9 Hz, 2H), 7.38-7.36 (d, *J* = 7.9 Hz, 2H), 7.20 (brs, 1H), 6.66 (s, 1H), 5.04 (brs, 1H), 4.59-4.55 (m, 1H), 4.04-4.02 (m, 1H), 3.93-3.91 (m, 1H), 3.74-3.66 (m, 2H), 3.53-3.48 (m, 1H), 2.17-2.15 (m, 1H), 2.00-1.98 (m, 1H).

3-((4-cyanophenyl)amino)-1-((3R,4S)-4-cyanotetrahydro-2H-pyran-3-yl)-1H-pyrazole-4-carboxamide (**22**). Prepared following similar procedure described for **28** in 20% yield). LRMS (ESI) calcd for ($C_{17}H_{16}N_6O_2$) $[M + H]^+$ 337.1, found 337.1. HRMS: calcd for ($C_{17}H_{16}N_6O_2$) $[M + H]^+$ 337.1413, found 337.1388; difference 7.4 ppm. ^{1}H NMR (500 MHz, DMSO-d_6) δ 9.64 (s, 1H), 8.33 (s, 1H), 7.82 (brs, 1H), 7.66 (s, 4H), 7.29 (brs, 1H), 4.63-4.58 (m, 1H), 4.03-4.00 (m, 1H), 3.90-3.88 (m, 1H), 3.71-3.64 (m, 2H), 3.50-3.46 (m, 1H), 2.15-2.13 (m, 1H), 2.01-1.93 (m, 1H). ^{13}C NMR (500 MHz, DMSO-d_6): δ 166.1, 151.9, 145.4, 133.9 (2C), 131.9, 120.25, 120.14, 116.8 (2C), 102.2, 101.2, 69.3, 65.4, 58.1, 31.8, 28.4. $[\alpha]_D^{20}$ +144 (*c* 0.37, MeOH/DMSO 1:1).

1-((3R,4S)-4-cyanotetrahydro-2H-pyran-3-yl)-3-((2,3-dimethyl-1,1-dioxido-2,3-dihydrobenzo[d]isothiazol-5-yl)amino)-1H-pyrazole-4-carboxamide (**23**). Prepared following similar procedure described for **28** in 61% yield. LRMS (ESI) calcd for ($C_{19}H_{22}N_6O_4S$) $[M + H]^+$ 431.1, found 431.1. HRMS: calcd for ($C_{19}H_{22}N_6O_4S$) $[M + H]^+$ 431.1501, found 431.1498; difference 0.7 ppm. ^{1}H NMR (500 MHz, DMSO-d_6) δ 9.64 (s, 1H), 8.34 (s, 1H), 7.81 (brs, 1H), 7.75 (s, 1H), 7.72-7.70 (d, *J* = 8.7 Hz, 1H), 7.67-7.65 (d, *J* = 8.0 Hz, 1H), 7.30 (brs, 1H), 4.64-4.59 (m, 1H), 4.32-4.28 (m, 1H), 4.06-4.04 (m, 1H), 3.92-3.89 (m, 1H), 3.71-3.64 (m, 2H), 3.49-3.38 (m, 1H), 2.51-2.42 (m, 1H), 2.48 (s, 3H), 2.16-2.13 (m, 1H), 2.02-1.94 (m, 1H), 1.48-1.47 (d, *J* = 6.1 Hz, 3H).

3-((4-cyano-3-methoxyphenyl)amino)-1-((3R,4S)-4-cyanotetrahydro-2H-pyran-3-yl)-1H-pyrazole-4-carboxamide (**24**). Prepared following similar procedure described for **28** in 49% yield. LRMS (ESI) calcd for ($C_{18}H_{18}N_6O_3$) $[M + H]^+$ 467.1, found 467.1. ^{1}H NMR (500 MHz, DMSO-d_6) δ 9.62 (s, 1H), 8.34 (s, 1H), 7.82 (brs, 1H), 7.51-7.50 (d, *J* = 7.7 Hz, 1H), 7.51 (s, 1H), 7.30 (brs, 1H), 7.17-7.15 (d, *J* = 8.3 Hz, 1H), 4.65-4.60 (m, 1H), 4.05-3.99 (m, 2H), 3.92 (s, 3H), 3.69-3.62 (m, 2H), 3.44-3.40 (m, 1H), 2.15-2.13 (m, 1H), 2.01-1.93 (m, 1H).

3-((4-cyano-3-cyclopropylphenyl)amino)-1-((3R,4S)-4-cyanotetrahydro-2H-pyran-3-yl)-1H-pyrazole-4-carboxamide (**25**). Prepared following similar procedure described for **28** in 40% yield. LRMS (ESI) calcd for ($C_{20}H_{20}N_6O_2$) $[M + H]^+$ 377, found 377. HRMS: calcd for ($C_{20}H_{20}N_6O_2$) $[M + H]^+$ 377.1726, found 377.1701; difference 6.6 ppm. ^{1}H NMR (500 MHz, DMSO-d_6) δ 9.50 (s, 1H), 8.33 (s, 1H), 7.80 (brs, 1H), 7.58-7.56 (d, *J* = 8.5 Hz, 1H), 7.52-7.50 (d, *J* = 8.3 Hz, 1H), 7.28 (brs, 1H), 7.19 (s, 1H), 4.64-4.60 (m, 1H), 4.07-4.04 (m, 1H), 3.94-3.92 (m, 1H), 3.67-3.60 (m, 2H), 3.47-3.42 (m, 1H), 2.18-2.09 (m, 2H), 2.02-1.96 (m, 1H), 1.11-1.09 (d, *J* = 8.2 Hz, 2H), 0.88-0.81 (m, 2H).

1-((3R,4S)-4-cyanotetrahydro-2H-pyran-3-yl)-3-((3,4-dicyanophenyl)amino)-1H-pyrazole-4-carboxamide (**26**). Prepared in analogy to that described for **28** in 16% yield. LRMS (ESI) calcd for

($C_{18}H_{15}N_7O_2$) [M + H]$^+$ 362, found 362. HRMS: calcd for ($C_{18}H_{15}N_7O_2$) [M + H]$^+$ 362.1365, found 362.1352; difference 3.6 ppm. ^{1}H NMR (500 MHz, DMSO-d_6) δ9.89 (s, 1H), 8.39 (s, 1H), 8.19 (s, 1H), 8.08-8.07 (d, *J* = 8.3 Hz, 1H), 7.94-7.93 (d, J = 8.8 Hz, 1H), 7.87 (brs, 1H), 7.37 (brs, 1H), 4.68-4.68 (m, 1H), 4.07-4.04 (m, 1H), 3.94-3.90 (m, 1H), 3.74-3.66 (m, 2H), 3.52-3.47 (m, 1H), 2.18-2.14 (m, 1H), 2.04-1.95 (m, 1H).

3-((3-chloro-4-cyanophenyl)amino)-1-((3R,4S)-4-cyanotetrahydro-2H-pyran-3-yl)-1H-pyrazole-4-carboxamide (**27**). Prepared following similar procedure described for **28** in 45% yield. LRMS (ESI) calcd for ($C_{17}H_{15}ClN_6O_2$) [M + H]$^+$ 371.1, found 371.1. HRMS: calcd for ($C_{17}H_{15}ClN_6O_2$) [M + H]$^+$ 371.1023, found 371.1003; difference 5.4 ppm. ^{1}H NMR (500 MHz, DMSO-d_6) δ 9.75 (s, 1H), 8.36 (s, 1H), 7.89 (s, 1H), 7.84 (brs, 1H), 7.76-7.74 (d, *J* = 8.6 Hz, 1H), 7.65-7.63 (d, *J* = 8.6 Hz, 1H), 7.33 (brs, 1H), 4.66-4.61 (m, 1H), 4.05-4.02 (m, 1H), 3.92-3.88 (m, 1H), 3.68-3.62 (m, 2H), 3.49-3.45 (m, 1H), 2.16-2.13 (m, 1H), 2.02-1.93 (m, 1H).

3-((4-Chloro-3-methoxyphenyl)amino)-1-((3*R*,4*S*)-4-cyanotetrahydro-2*H*-pyran-3-yl)-1*H*-pyrazole-4-carboxamide (28)

A 500 mL 3-neck flask was fitted with a reflux condenser and J-KEM thermocouple, then charged with 3-amino-1-((3*R*,4*S*)-4-cyanotetrahydro-2*H*-pyran-3-yl)-1*H*-pyrazole-4-carboxamide (10.0 g, 42.5 mmol), 5-bromo-2-chloroanisole (14.1 g, 63.7 mmol), potassium acetate (6.26 g, 63.8 mmol) and 2-propanol (150 ml). The reactions mixture was purged with nitrogen gas for 20 min, then $Pd_2(dba)_3$ (1.95 g, 2.13 mmol) and 2-di-*tert*-butylphosphino-2',4',6'-triisopropylbiphenyl (2.00 g, 4.71 mmol) were added. The reaction mixture was then heated to 80 ºC for 16.5 h. After cooling to 23 °C, acetone (150 mL) was added and the mixture was stirred for 10 min, then filtered through celite with acetone elution. The filtrate was concentrated onto silica gel in vacuo and purified via flash-column chromatography (ISCO 220g cartridge, gradient elution with 3–6% methanol-dicholoromethane). The product-containing fractions were concentrated to afford 3-

((4-chloro-3-methoxyphenyl)amino)-1-((3*R*,4*S*)-4-cyanotetrahydro-2*H*-pyran-3-yl)-1*H*-pyrazole-4-carboxamide (12.2 g, 30.7 mmol, 72.3 % yield) as a bright yellow solid.

LRMS (ESI) calcd for $C_{17}H_{19}ClN_5O_3$ $[M+H]^+$: 376, Found: 376. HRMS: calcd mass for $C_{17}H_{19}ClN_5O_3$ $[M+H]^+$ 376.1176; found 376.1163; difference 3.5 ppm. ^{1}H NMR (600 MHz, DMSO-d6): δ 9.24 (s, 1H), 8.31 (s, 1H), 7.75 (s, 1H), 7.48 (d, *J* = 2.3 Hz, 1H), 7.23-7.22 (m, 2H); 7.08 (dd, *J* = 8.6, 2.3 Hz, 1H), 4.59 (td, *J* = 10.2, 4.4 Hz, 1H), 4.05 (dd, *J* = 11.3, 4.4 Hz, 1H), 3.94-3.87 (m, 4H), 3.68-3.64 (m, 2H), 3.44 (t, *J* = 11.7 Hz, 1H), 2.16 (d, *J* = 13.3 Hz, 1H), 1.98 (qd, *J* = 12.3, 4.3 Hz, 1H). ^{13}C NMR (500 MHz, DMSO-d_6): δ 166.3, 155.2, 152.7, 141.9, 131.7, 130.2, 120.2, 111.4, 109.4, 101.54, 101.52, 69.5, 65.9, 58.0, 56.2, 32.0, 2 8.5. $[\alpha]_D^{20}$ +136 (*c* 0.74, MeOH).

1-((3R,4S)-4-cyanotetrahydro-2H-pyran-3-yl)-3-((2-(dimethylamino)-6-fluoropyridin-4-yl)amino)-1H-pyrazole-4-carboxamide (**29**). Prepared following similar procedure described for **28** in 27% yield. LRMS (ESI) calcd for ($C_{17}H_{20}FN_7O_2$) $[M + H]^+$ 374.1, found 374.1. HRMS: calcd for ($C_{17}H_{20}FN_7O_2$) $[M + H]^+$ 374.1741, found 374.1756; difference -4.0 ppm. ^{1}H NMR (500 MHz, DMSO-d_6) δ 9.47 (s, 1H), 8.31 (s, 1H), 7.79 (brs, 1H), 7.27 (brs, 1H), 6.53 (s, 1H), 6.46 (s, 1H), 4.62-4.58 (m, 1H), 4.05-3.99 (m, 1H), 3.91-3.88 (m, 1H), 3.65-3.59 (m, 2H), 3.45-3.40 (m, 1H), 2.97 (s, 6H), 2.16-2.12 (m, 1H), 2.00-1.93 (m, 1H).

1-((3R,4S)-4-cyanotetrahydro-2H-pyran-3-yl)-3-((2-fluoro-6-methoxypyridin-4-yl)amino)-1H-pyrazole-4-carboxamide (**30**). Prepared following similar procedure described for **28** in 27% yield. LRMS (ESI) calcd for ($C_{16}H_{17}FN_6O_3$) $[M + H]^+$ 361.1, found 361.1. HRMS: calcd for ($C_{16}H_{17}FN_6O_3$) $[M + H]^+$ 361.1424, found 361.1394; difference 8.3 ppm. ^{1}H NMR (500 MHz, DMSO-d_6) δ9.68 (s, 1H), 8.34 (s, 1H), 7.82 (brs, 1H), 7.31 (brs, 1H), 6.86 (s, 1H), 6.83 (s, 1H), 4.65-4.60 (m, 1H), 4.03-4.00 (m, 1H), 3.91-3.87 (m, 1H), 3.78 (s, 3H), 3.68-3.60 (m, 2H), 3.50-3.45 (m, 1H), 2.16-2.12 (m, 1H), 2.00-1.92 (m, 1H).

1-((3R,4S)-4-cyanotetrahydro-2H-pyran-3-yl)-3-((8-fluoro-4-methoxyquinolin-6-yl)amino)-1H-pyrazole-4-carboxamide (**31**). Prepared following similar procedure described for **28** in 23% yield. LRMS

(ESI) calcd for ($C_{20}H_{19}FN_6O_3$) $[M + H]^+$ 411.1, found 411.1. HRMS: calcd for ($C_{20}H_{19}FN_6O_3$) $[M + H]^+$ 411.1581, found 411.1596; difference -3.6 ppm. ^{1}H NMR (500 MHz, DMSO-d_6) δ 9.54 (s, 1H), 8.55-8.54 (d, *J* = 4.3 Hz, 1H), 8.35 (s, 1H), 8.11 (s, 1H), 7.86-7.84 (d, *J* = 13.5 Hz, 1H), 7.80 (brs, 1H), 7.28 (brs, 1H), 7.02-7.01 (d, *J* = 4.5 Hz, 1H), 4.68-4.62 (m, 1H), 4.11-4.08 (m, 1H), 4.05 (s, 3H), 3.98-3.94 (m, 1H), 3.73-3.69 (m, 1H), 3.67-3.64 (m, 1H), 3.51-3.46 (m, 1H), 2.24-2.20 (m, 1H), 2.05-1.98 (m, 1H).

3-((4-chloro-8-fluoroquinolin-6-yl)amino)-1-((3R,4S)-4-cyanotetrahydro-2H-pyran-3-yl)-1H-pyrazole-4-carboxamide (**32**). Prepared following similar procedure described for **28,** yield not determined. LRMS (ESI) calcd for ($C_{19}H_{16}ClFN_6O_3$) $[M + H]^+$ 415.1, found 415.1. HRMS: calcd for ($C_{19}H_{16}ClFN_6O_3$) $[M + H]^+$ 415.1085, found 415.1090; difference -1.2 ppm. ^{1}H NMR (500 MHz, DMSO-d_6) δ 9.66 (s, 1H), 8.61 (d, *J* = 3.6 Hz, 1H), 8.44 (s, 1H), 8.38 (s, 1H), 7.89-7.86 (d, *J* = 12.7 Hz, 1H), 7.85 (brs, 1H), 7.76 (d, *J* = 3.4 Hz, 1H), 7.31 (brs, 1H), 4.71-4.66 (m, 1H), 4.13-4.10 (m, 1H), 3.97-3.95 (m, 1H), 3.76-3.71 (m, 1H), 3.67-3.63 (m, 1H), 3.46-3.41 (m, 1H), 2.23-2.21 (m, 1H), 2.05-1.98 (m, 1H).

1-((3R,4S)-4-cyanotetrahydro-2H-pyran-3-yl)-3-((4-methylquinazolin-6-yl)amino)-1H-pyrazole-4-carboxamide (**33**).

Prepared following similar procedure described for **28** in 38% yield. LRMS (ESI) calcd for ($C_{19}H_{19}N_7O_2$) $[M + H]^+$ 378.1, found 378.1. HRMS: calcd for ($C_{19}H_{19}N_7O_2$) $[M + H]^+$ 378.1678, found 378.1673; difference 1.3 ppm. ^{1}H NMR (500 MHz, DMSO-d_6) δ 9.67 (s, 1H), 8.98 (s, 1H), 8.60-8.59 (d, *J* = 2.4 Hz, 1H), 8.38 (s, 1H), 8.06-8.04 (dd, *J* = 9.1, 2.4 Hz, 1H), 7.91-7.89 (d, *J* = 9.1 Hz, 1H), 7.85 (brs, 1H), 7.32 (brs, 1H), 4.71-4.66 (m, 1H), 4.14-4.10 (m, 1H), 3.98-3.94 (m, 1H), 3.78-3.72 (m, 2H), 3.48-3.44 (m, 1H), 2.94 (s, 3H), 2.21-2.17 (m, 1H), 2.06-1.98 (m, 1H).

<u>Aromatic building block synthesis</u>

Synthesis of 5-bromo-2,3-dimethyl-2,3-dihydrobenzo[d]isothiazole 1,1-dioxide.

Step 1: 4-bromo-2-ethylbenzenesulfonyl azide. A solution of 4-bromo-2-ethylbenzene-1-sulfonyl chloride

(256 mg, 0.868 mmol) in water:acetone (1:1, 5.3 mL) was stirred in a 25 mL round bottom flask and cooled to 0 °C. Sodium azide (85 mg, 1.3 0 mmol) was added to the sulfonyl chloride mixture and the reaction was stirred and warm most of the acetone. The product was extracted from the aqueous layer using dichloromethane (3 x 20 mL). The organic layers were combined, washed with brine, dried over sodium sulfate, and concentrated in vacuo. The resulting colorless oil was purified by flash chromatography (9:1 hexanes/EtOAc). The pure fractions were combined and concentrated to afford the desired product in 83% yield. ^{1}H NMR (500 MHz, $CDCl_3$) δ 7.91-7.88 (dd, *J* = 8.3, 3.5 Hz, 1H), 7.62 (s, 1H), 7.56-7.53 (m, 1H), 3.04-3.00 (m, 2H), 1.35-1.31 (m, 3H).

Step 2: 5-bromo-3-methyl-2,3-dihydrobenzo[d]isothiazole 1,1-dioxide. An oven dried 2 mL vial with stir bar was evacuated and backfilled with argon (3x). Upon cooling to room temperature, 4-bromo-2-ethylbenzenesulfonyl azide (77 mg, 0.256 mmol) was added followed by chlorobenzene (1.3 mL) and 5 A MS. Co(II) meso-tetraphenylporphine (8.9 mg, 0.013 mmol) was then added and the reaction mixture was heated to 80 °C overnight. The reaction mixture was cooled to room temperature and purified by silica gel flash chromatography on ISCO, 5% EtOAc in hexanes to 50% EtOAc in hexanes gradient. Isolated 80% yield (56 mg) of the desired product. ^{1}H NMR (500 MHz, $CDCl_3$) δ 7.65-7.64 (d, *J* = 8.3 Hz, 1H), 7.62-7.60 (d, *J* = 8.3 Hz, 1H), 7.54 (s, 1H), 4.77-4.73 (q, *J* = 6.6 Hz, 1H), 1.61-1.60 (d, *J* = 6.5 Hz, 3H).

Step 3: 5-bromo-2,3-dimethyl-2,3-dihydrobenzo[d]isothiazole 1,1-dioxide. To a solution of 5-bromo-3-methyl-2,3-dihydrobenzo[d]isothiazole 1,1-dioxide (56 mg, 0.214 mmol) in DMF (0.7 mL) at 0 °C, NaH (60%) (8.5 mg, 0.214 mmol) was added. The reaction mixture was stirred for 15 minutes followed by the addition of iodomethane (17 µL, 0.267 mmol). The reaction was slowly warmed to room temperature overnight. The reaction was quenched with 1:1 sat. NH_4Cl/H_2O and diluted with Et_2O. The aqueous layer was extracted with Et_2O (3x20 mL). The combined organics were washed with brine, dried over Na_2SO_4, and concentrated in vacuo. The reaction mixture was purified by silica gel flash purification using 0% EtOAc - 30% EtOAc gradient afforded the desired product in 75% yield (44 mg). ^{1}H NMR (500 MHz, $CDCl_3$) δ 7.67 (s, 2H), 7.56 (s, 1H), 4.32-4.28 (q, *J* = 6.5 Hz, 1H), 2.91 (s, 3H), 1.56-1.55 (d, *J* = 6.6 Hz,

3H).

4-bromo-6-fluoro-*N,N*-dimethylpyridin-2-amine. Dimethylamine (2M in THF) (147 µl, 0.294 mmol) was added to a solution of 4-bromo-2,6-difluoropyridine (57 mg, 0.294 mmol) in THF (1 mL) at room temperature. The reaction was stirred for 30 min until TLC showed full conversion. The crude reaction mixture was concentrated and carried on forward without further purification 80% yield. ^{1}H NMR (500 MHz, $CDCl_3$) δ 6.44 (s, 1H), 6.29-6.28 (m, 1H), 3.06 (s, 6H).

6-bromo-8-fluoro-4-methoxyquinoline. To a microwave vial was added 6-bromo-4-chloro-8-fluoroquinoline (0.2 g, 0.768 mmol) and sodium methoxide (0.5 M in MeOH) (3.84 ml, 1.92 mmol). The vial was sealed and heated to 80 ºC for 2 hours. The mixture was cooled to room temperature, diluted with water, and extracted with EtOAc. The organic layer was dried over anhydrous magnesium sulfate and concentrated in vacuo. The residue was purified using flash silica gel chromatography with eluent gradient 10-100% EtOAc:Hex. Desired fractions were identified, combined, and concentrated in vacuo to afford the desired product in 77% yield. LRMS (ESI) calcd for ($C_{10}H_7BrFNO$) $[M + H]^+$ 256, found 256. ^{1}H NMR (500 MHz, $CDCl_3$) δ8.81-8.80 (d, J = 5.2, 1H), 8.16 (s, 1H), 7.54-7.52 (dd, J = 9.7, 2.0 Hz, 1H), 6.83-6.82 (d, J = 5.1 Hz, 1H), 4.07 (s, 3H).

Supporting Information

Kinase selectivity profile of key compounds in panel of 265 kinases and Table S1: Kinase selectivity for compounds **2**, **22**, **28**; JAK biochemical HTRF assay protocol; Cell based assay protocol; Human whole blood STAT phosphorylation assay protocol; Table S2: Crystallographic data collection and refinement statistics for the complex of JAK1 with compound **28;** Rat collagen induced arthritis (CIA) model; Experimental procedure for compounds **2, 3, 4, 5**; High-Throughput (HT) HPLC log D (pH 7.0) determination; High-Throughput (HT) FaSSIF solubility determination;

Hepatocyte intrinsic clearance method; Molecular formula strings; References.

Accession Codes

PDB code 5WO4. Authors will release the atomic coordinates and experimental data upon article publication.

Author Information

Corresponding Author

Tony Siu: phone, 617-992-2386, E-mail, tony_siu@merck.com

ORCID

Tony Siu: 0000-0001-5149-7457

Present Contact

Jason Brubaker, JBrubaker@blueprintmedicines.com

Joshua Close, jclose@blueprintmedicines.com

Hongbo Zeng, zeng.hongbo@gmail.com

Duan Liu, duan_liu@wuxiapptec.com

Dawn M. Mampreian, dawn.mampreian@modernatx.com

Nathan Bays, nathan.bays@lilly.com

Kevin Johnson, kevin.johnson@unumrx.com

Christopher J. Dinsmore, cdinsmore@formatherapeutics.com

Jonathan R. Young, jyoung@regulusrx.com

Notes

The authors declare no competing financial interest.

Acknowledgments:

T.S. thanks Jongwon Lim and Jared Cumming for careful reading of this manuscript and Bruce Adams and Bridget Becker for NMR support.

Abbreviations Used:

JAK, Janus Kinase; STAT, signal transducer and activator of transcription; RA, rheumatoid arthritis; DMARDS, disease modifying anti-rheumatic drugs; IL-6, interleukin-6; EPO, erythropoietin; Cl_{int}, intrinsic clearance; AUC_u, unbound area under the curve; f_a, fraction absorbed; f_g, fraction escaping gut metabolism; hERG, human ether-a-go-go-related gene; LBE, ligand binding efficiency; LLE, lipophilic ligand efficiency; SFC, super critical fluid chromatography; FASSIF, fasted state stimulated intestinal fluid; D_0, dose number; Cl_u, unbound clearance; IL-7, interleukin-7; QD, quaque die/everyday; ATP, adenosine triphosphate; CIA, collagen induced arthritis; PO, per os/by mouth; BID, bis in die/twice a day.

References:

1) Shuai, K.; Liu, B. Regulation of JAK-STAT signaling in the immune system. *Nat. Rev. Immunol.* **2003**, *3*, 900-910.

2) (a) Pesu, M.; Laurence, A.; Kishore, N.; Zwillich, S. H.; Chan, G.; O'Shea, J. J. Therapeutic targeting of janus kinases. *Immunol. Rev.* **2008**, *223*, 132−142. (b) O'Shea, J. J; Schwartz, D. M.; Villarino, A. V.; Gadina, M.; McInnes, I. B.; Laurence, A. The JAK-STAT pathway: impact on human disease and therapeutic intervention. *Annu. Rev. Med.* **2015,** *66,* 311-328.

3) Pisetsky, D. S.; Ward, M. M. Advances in the treatment of inflammatory arthritis. *Best Pract. Res. Clin. Rheumatol*. **2012**, *26*, 251-261.

4) (a) Kremer, J. M.; Bloom, B. J.; Breedveld, F. C.; Coombs, J. H.; Fletcher, M. P.; Gruben, D.; Krishnaswami, S.; Burgos-Vargas, R.; Wilkinson, B.; Zerbini, C. A.; Zwillich, S. H. The safety and efficacy of a JAK inhibitor in patients with active rheumatoid arthritis: results of a double-blind, placebo-controlled phase IIa trial of three dosage levels of CP-690,550 versus placebo. *Arthritis Rheum*. **2009**, *60*, 1895−1905. (b) Flanagan, M. E.; Blumenkopf, T. A.; Brissette, W. H.; Brown, M. F.; Casavant, J. M.; Shang-Poa, C.; Doty, J. L.; Elliot, E. A.; Fisher, M. B.; Hines, M.; Kent, C.; Kudlacz, E. M.; Lillie, B. M.; Magnuson, K. S.; McCurdy, S. P.; Munchhof, M. J.; Perry, B. D.; Sawyer, P. S.; Strelevitz, T. J.; Subramanyam, C.; Sun, J.; Whipple, D. A.; Changelian, P. S. Discovery of CP-690,550: a potent and selective janus kinase (JAK) inhibitor for the treatment of autoimmune diseases and organ transplant rejection. *J. Med. Chem.* **2010**, *53*, 8468-8484. (c) Kaur, K.; Kalra, S.; Kaushal, S. Systematic review of tofacitinib: a new drug for the management of rheumatoid arthritis. *Clin. Ther.* **2014**, *36*, 1074-1086.

5) Bathon, J. M.; Martin, R. W.; Fleischmann, R. M.; Tesser, J. R.; Schiff, M. H.; Keystone, E. C.; Genovese, M. C.; Wasko, M. C.; Moreland, L. W.; Weaver, A. L.; Markenson J.; Finck, B. K. A comparison of etanercept and methotrexate in patients with early rheumatoid arthritis. *N. Engl. J. Med.* **2000**, *343*, 1586-1593.

6) For an excellent review see: (a) Menet, C. J.; Mammoliti, O.; Lopez-Ramos, M. Progress toward JAK1-selective inhibitors. *Future Med. Chem.* **2015,** *7,* 203-235. For JAK1 Selective Inhibitors see: (b) Kulagowski, J. J.; Blair, W.; Bull, R. J.; Chang, C.; Deshmukh, G.; Dyke, H. J.; Eigenbrot, C.; Ghilardi, N.; Gibbions, P.; Harrison, T. K.; Hewitt, P. R.; Liimatta, M.; Hurley, C. A.; Johnson, A.; Johnson, T.; Kenny, J. R.; Kohli, P. B.; Maxey, R. J.; Mendonca, R.; Mortara, K.; Murray, J.; Narukulla, R.; Shia, S.; Steffek, M.; Ubhayakar, S.; Ultsch, M.; van Abbema, A.; Ward, S. I.; Waszkowycz, B.; Zak, M. Identification of imidazo-pyrrolopyridines as novel and potent JAK1 inhibitors. *J. Med. Chem.* **2012**, *55*, 5901-5921. (c) Zak, M.; Mendonca, R.; Balazas, M.; Barrett, K.;

Bergeron, P.; Blair, W. S.; Chang; C.; Deshmukh, G.; DeVoss, J.; Dragovish, P. S.; Eigenbrot, C.; Ghilardi, N.; Bibbons, P.; Gradl, S.; Hamman, C.; Hanan, E. J.; Harstad, E.; Hewitt, P. R.; Hurley, C. A.; Jin, T.; Johnson, A.; Johnson, T.; Kenny, J. R.; Koehler, M. F. T.; Kohli, P. B.; Kulagowski, J. J.; Labadie, S.; Liao, J.; Liimatta, M.; Lin, Z.; Lupardus, P. J.; Maxey, R. J.; Murray, J. M.; Pulk, R.; Rodriguez, M.; Savage, S.; Shia, S.; Streffek, M.; Ubhayakar, S.; Ultsch, M.; van Abbema, A.; Ward, S. I.; Xiao, L.; Xiao, Y. Discovery and optimization of *C*-2 methyl imidazopyrrolopyridines as potent and orally bioavaliable JAK1 inhibitors with selectivity over JAK2. *J. Med. Chem.* **2012**, *55*, 6176-6193. (d) Zak, M.; Hurley, C. A.; Ward, S. I.; Bergeron, P.; Barrett. K.; Balazs, M.; Blair, W. S.; Bull, R.; Charkravarty, P.; Chang, C.; Crackett, P.; Deshmukh, G.; DeVoss, J.; Dragovich, P. S.; Eigenbrot, C.; Ellwood, C.; Gaines, S.; Ghilardi, N.; Gibbons, P.; Gradl, S.; Gribling, P.; Hamman, C.; Harstad, E.; Hewitt, P.; Johnson, A.; Johnson, T.; Kenny, J. R.; Koehler M. F. T.; Kohli P. B.; Labadie, S.; Lee, W. P.; Liao, J.; Limatta, M.; Mendonca, R.; Narukulla, R.; Pulk, R.; Reeve, A.; Savage, S.; Shia, S.; Steffek, M.; Ubhayakar, S.; van Abbema, A.; Aligas, I.; Avitabile-Woo, B.; Xiao, Y.; Yang, J. Kulagowski J. J. Identification of C-2 hydroyethyl imidazopyrrolopyridines as potent JAK1 inhibitors with favorable physicochemical properties and high selectivity over JAK2. *J. Med. Chem.* **2013**, *56*, 4764-4785. (e) Menet, C. J.; Fletcher, S. R.; Van Lommen, G.; Geney, R.; Blanc, J.; Smits, K.; Jouannigot, N.; Deprez, P.; van der Aar, E. M.; Clement-Lacriox, P.; Lepescheux, L.; Galien R.; Vayssiere, B.; Nelles, L.; Christopher, T.; Brys, R.; Uhring, M. Ciesielski, F.; Van Rompaey, L. Triazolopyridines as selective JAK1 inhibitors: from hit identification to GLPG0634, *J. Med. Chem.* **2014**, *57*, 9323-9342. (f) Kim, M. K.; Shin H.; Park, K.; Kim H.; Park, J.; Kim, K.; Nam, J.; Choo, H.; Chong Y. Benzoimdazole derivatives as potent JAK1 selective inhibitors. *J. Med. Chem*. **2015**, *58*, 7596-7602. (g) Simov, V.; Deshmukh, S. V.; Dinsmore, C. J.; Elwood, F.; Fernandez, R. B.; Garcia, Y.; Gibeau, C.; Gunaydin, H.; Jung, J.; Katz, J. D.; Kraybill, B.; Lapointe, B.; Patel, S. B.; Siu, T.; Su, H.; Young, J. R. Structure-based design and development of (benz)imidazole pyridones as JAK1-selective kinase Inhibitors. *Bioorg. Med. Chem. Lett.* **2016**, *26*, 1803-1808. (h) For a review of JAK

inhibitors in the clinic see: Roskoski Jr., R. Janus kinase (JAK) inhibitors in the treatment of inflammatory and neoplastic diseases. *Pharmacol. Res.* **2016**, *111*, 784-803.

7) Brubaker, J. Discovery of an orally bioavailable JAK1 inhibitor for validation of JAK1-selective hypothesis. Presented at Applied Pharmaceutical Chemistry Conference, Boston, Massachusetts, March 4, 2014.

8) Moy, L.; Chiu C-S.; Faltus, R.; Zielstorff, M.; Chakravarthy, K.; Deshmukh, S.; Kariv, I.; Klappenbach, J.; Brubaker, J.; Liu, D.; Siu, T.; Young, J.; Yu, H.; Elwood, F.; Cicmil, M. Efficacy of a novel orally bioavailable JAK1 selective compound in a preclinical rat collagen-induced arthritis model. Presented at ACR/ARHP Annual Meeting, Boston, Massachusetts, November 14-19, 2014.

9) Human dose predication was based achieving exposure needed to achieve 15% pit improvements in ACR50 over 10 mg BID Tofacitinib. PK/PD modeling for the required exposure will be disclosed in a future publication.

10) (a) Dack, K. Reducing Attrition Risk: Evolution of an in silico "compound safety evaluator" designing safer medicines in discovery. SCI, London March 17, 2011. (b) Uetrecht, J.; Idiosyncratic drug reactions: current understanding. *Annu. Rev. Pharmacol. and Toxicol.* **2007**, *47*, 513-539. (c) Chalasani, N.; Bjornsson, E. Risk factors for idiosyncratic drug-induced liver injury. *Gastroenterology* **2010**, *138*, 2246-2259. (d) Tujios, S.; Fontana, R. J.; Mechanisms of drug-induced liver injury from bedside to bench. *Nat. Rev. Gastroenterol. Hepatol.* **2011**, *8*, 202-211.

11) (a) Oh, D.; Curl, R. L.; Amidon, G. L. Estimating the fraction dose absorbed from suspensions of poorly soluble compounds in humans: a mathematical model. *Pharm. Res.* **1993**, *10*, 264-270. (b)

Dahan, A.; Miller J. M.; Amidon, G. L. Prediction of solubility and permeability class membership: provisional BCS classification of the world top oral drugs. *AAPS J.* **2009**, *11*, 740-746.

12) Kerns, E. H.; Di, Li. *Drug-Like Properties: Concepts, Structure Design and Methods: from ADME to Toxicity Optimization*; Academic Press: San Diego, 2008; pp 223.

13) The MK499 IC_{50} values were acquired by radio ligand binding competition experiments using membrane preparations from human embryonic kidney cells that express hERG. IC_{50} values are reported as the averages of at least two independent determinations; standard deviations are within +/- 25-50% of IC_{50} values. For assay detail see Bell, I. M.; Gallicchio, S. N.; Abrams, M.; Beshore, D. C.; Buser, C. A.; Culberson, J. C.; Davide, J.; Ellis-Hutchings, M.; Fernandes C.; Gibbs, J. B.; Graham, S. L.; Hartman, G. D.; Heimbrook, D. C.; Homnick, C. F.; Huff, J. R.; Kassahun, K.; Koblan, K. S.; Kohl, N. E.; Lobell, R. B.; Lynch Jr.; J. J.; Miller, P. A.; Omer, C. A.; Rodrigues, A. D.; Walsh, E. S.; Williams, T. M. Design and biological activity of (*S*)-4-{[1-(3-chlorobenzyl-2-oxopyrrolidin-3-ylamino]methyl}imidazol-1-ylmethylbenzonitrile, a 3-Aminopyrrolidine farnesyltransferase inhibitor with excellent cell potency. *J. Med. Chem.* **2001**, *44*, 2933-2949 and references therein.

14) (a) Redfern, W. S.; Carlsson, L.; Davis, A. S.; Lynch, W. G.; MacKenzie, I.; Palethorpe, S.; Sieql, P.K. S; Strang, A. T.; Sullivan, A. T.; Wallis, R.; Camm, A. J.; Hammond, T. G. Relationship between preclinical cardiac electrophysiology, clinical QT interval prolongation and Torsade de Pontes for a broad range of drugs: evidence for provisional safety margin in drug development. *Cardiovasc. Res.* **2003** *58* 32-45. (b) Trepakova, E. S.; Malik, M. G.; Imredy, J. P.; Penniman, J. R.; Dech, S. J.; Salata, J. J. Application of PatchXpress planar patch clamp technology to the screening of new drug candidates for cardiac KCNQ1/KCNE1 (I Ks) activity. *Assay and Drug Dev. Technol.* **2007**, *5*, 617–627. (c) Morissette, P.; Nishida, M.; Trepakova, E.; Imredy J.; Lagrutta, A.; Chaves, A.; Hoagland, K.; Hoe, C. L.; Zrada, M. M.; Travis, J. J.; Zingaro, G. J.; Gerenser, P.; Friedrichs, G.; Salata, J. J. The

anesthetized guinea pig: an effective early cardiovascular derisking and lead optimization model. *J. Pharmacol. Toxicol. Methods* **2015**, *68*, 137-149.

15) (a) Fermini, B.; Fossa, A. A. The impact of drug-induced QT interval prolongation on drug discovery and development. *Nat. Rev. Drug Discovery* **2003**, *2*, 439-447. (b) Roden, D. M. Drug-induced prolongation of the QT interval. *N. Engl. J. Med.* **2004**, *350*, 1013-1022.

16) (a) Cavalli, A.; Poluzzi, E.; De Ponti, F.; Recanatini, M. Toward a pharmacophore for drugs inducing the long QT syndrome: insights from a CoMFA study of HERG K^+ channel blockers. *J. Med. Chem.* **2002**, *45*, 3844-3853. (b) Jamieson, C.; Moir, E. M.; Rankovic, Z.; Wishart, G. Medicinal Chemistry of hERG optimizations: highlights and hang-ups. *J. Med. Chem*. **2006**, *49*, 5029-5046.

17) (a) Hopkins, A. L.; Groom, C. R.; Alex, A. Ligand efficiency: A useful metric for lead selection. *Drug Discovery Today* **2004**, *9*, 430−431. (b) Abad-Zapatero, C. Ligand efficiency indices for effective drug discovery. *Expert Opin. Drug Discovery* **2007**, *2*, 469-488.

18) Meanwell, N. A. Improving drug candidates by design: a focus on physicochemical properties as a means of improving compound disposition and safety. *Chem. Res. Toxicol.* **2011**, *24*, 1420-1456.

19) (a) Leeson, P. D.; Springthorpe, B. The influence of drug-like concepts on decision making in medicinal chemistry. *Nat. Rev. Drug Discovery* **2007**, *6*, 881-890. (b) Edwards, M. P.; Price, D. A. role of physicochemical properties and ligand lipophilicity in addressing drug safety risks. *Annu. Rep. Med. Chem*. **2010**, *45*, 381-391. (c) Tarcsay, A.; Nyiri, K.; Keseru, G. M. Impact of lipophilic efficiency on compound quality. *J. Med. Chem.* **2012**, *55*, 1252−1260.

20) Anderson, K. W.; Tundel R. E.; Ikawa, T.; Altman, R.A.; Buchwald, S. L. Monodentate phosphines provide highly active catalysts for Pd-catalyzed C-N bond-forming reactions of heteroaromatic halides/amines and (H)N-heterocycles. *Angew. Chem. Int. Ed. Engl*. **2006**, *45*, 6523–6527.

21) Figures 6 and 7 were generated using Tibco Spotfire 7.0.1 (spotfire.tibco.com).

22) (a) van de Waterbeemd, H.; Smith, D. A.; Beaumont, K.; Walker, D. K. Property-based design: optimization of drug absorption and pharmacokinetics. *J. Med. Chem.* **2001**, *44*, 1313-1333. (b) van de Waterbeemd, H.; Smith, D. A.; Jones, B. C. Lipophilicity in pk design: methyl, ethyl, futile. *J. Comput.-Aided Mol. Des.* **2001**, *15*, 273–286. (c) Leeson, P. D.; Davis, A. M. Time-related differences in the physical property profiles of oral drugs. *J. Med. Chem.* **2004**, *47*, 6338–6348. (d) Lazerwith, S. E.; Bahador G.; Canales, E.; Cheng, G.; Chong, L.; Clarke, M. O.; Doerffler, E.; Eisenberg, E. J.; Hayes, J.; Lu, B.; Liu, Q.; Matles, M.; Mertzman, M.; Mitchell, M. L.; Morganelli, P.; Murray, B. P.; Robinson, M.; Strickley, R. G.; Tessler, M.; Tirunagari, N.; Wang, J.; Wang, Y.; Zhang, J. R.; Zheng, X.; Zhong, W.; Watkins, W. J. Optimization of pharmacokinetics through manipulation of physicochemical properties in a series of HCV inhibitors. *ACS Med. Chem. Lett.* **2011**, *2*, 715–719.

23) Fleming F. F.; Yao, L.; Ravikumar, P. C.; Funk, L.; Shook, B. C. Nitrile-containing pharmaceuticals: efficacious roles of the nitrile pharmacophore. *J. Med. Chem.* **2010**, *53*, 7902–7917.

24) Selectivity folds were calculated based on estimated IC_{50}'s from 3 point titrations (1, 100, 1000 nM) and the internal JAK1 potencies. 265 kinases were screened at a Invitrogen at their respective K_M. For the full list of kinases, see supporting information.

25) Cheng, A. C.; Eksterowicz J.; Geuns-Meyer S.; Sun, Y. Analysis of kinase inhibitor selectivity using a thermodynamics-based partition index. *J. Med. Chem.* **2010**, *53*, 4502-4510.

26) JAK1 kinase domain at 20 mg/mL was incubated with 1.6 mM adenosine and 3.2 mM DTT for 60 minutes then crystallized at 4°C using vapor diffusion. Equal volumes of protein and reservoir were mixed and suspended over a 1 mL reservoir containing 30%w/v polyethylene glycol 6000 and 100 mM MES buffer at pH 6.3. After streak-seeding, crystals appeared within 3 days. Crystals were soaked with 4 mM **28** for 5 days prior to flash cooling. Synchrotron data were collected at the Canadian Light Source [Grochulski, P., Fodje, M.N., Gorin, J., Labiuk, S.L. and Berg, R. (2011) Beamline 08ID-1, the prime beamline of the Canadian Macromolecular Crystallography Facility. *J. Synchrotron Rad*. **18**, 681-684]. Data collection and refinement details are found in Table S2. Coordinates have been deposited with PDB code 5WO4. Figures 9 and 10 were generated using PyMOL (The PyMOL Molecular Graphics System, Schrödinger, LLC).

27) JAK2 PDB 3LPB

28) View Contacts version 2.24, Desert Scientific Software, Norwest, Australia

29) Courtenay, J.S.; Dallman, M.J.; Dayan, A.D.; Martin, A.; Mosedale, B. Immunization against heterologous type II collagen induces arthritis in mice. *Nature* **1980**, *283*, 666–668 (1980).

30) Figure 11 was generated using Prism 7 (https://www.graphpad.com/scientific-software/prism/)

Table of Content Graphics

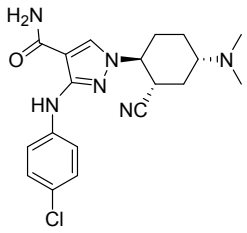

2

Cell IC_{50} EPO/IL6 = 11 X
Predicted Human Dose = 343 mg QD
D_0 = 80

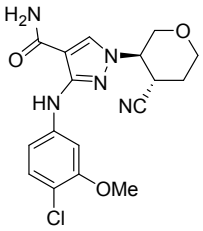

28

Cell IC_{50} EPO/IL6 = **25 X**
Predicted Human Dose = **81 mg QD**
D_0 = **25**

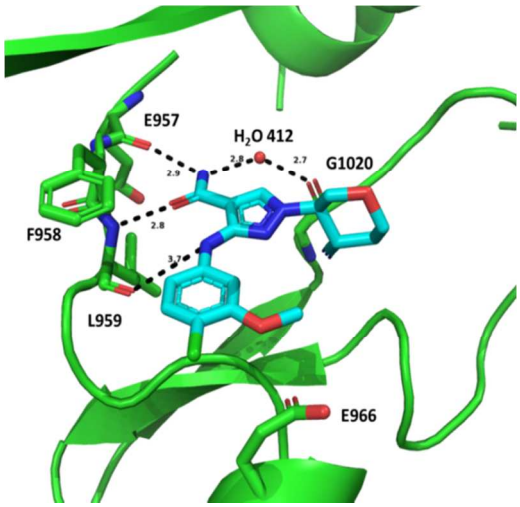

Compound 28 bound to JAK1 Protein